

# A Reluctance Actuator Gap Disturbance Testbed

by

Roberto J. Meléndez H.

B.S., Massachusetts Institute of Technology (2012)

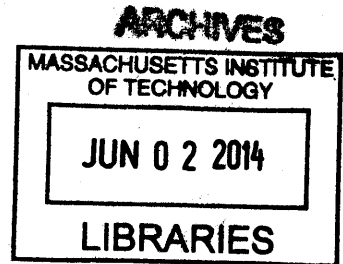
Submitted to the Department of Mechanical Engineering  
in partial fulfillment of the requirements for the degree of

Masters of Science in Mechanical Engineering

at the

MASSACHUSETTS INSTITUTE OF TECHNOLOGY

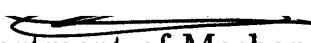
June 2014



© Massachusetts Institute of Technology 2014. All rights reserved.

Signature redacted

Author .....

  
Department of Mechanical Engineering  
May 9th, 2014

Signature redacted

Certified by .....

David L. Trumper  
Professor of Mechanical Engineering  
Thesis Supervisor

Signature redacted

Accepted by .....

David E. Hardt  
Chairman, Department Committee on Graduate Students  
Ralph E. and Eloise F. Cross Professor of Mechanical Engineering



# **A Reluctance Actuator Gap Disturbance Testbed**

by

**Roberto J. Meléndez H.**

Submitted to the Department of Mechanical Engineering  
on May 9th, 2014, in partial fulfillment of the  
requirements for the degree of  
Masters of Science in Mechanical Engineering

## **Abstract**

We have designed and built a Reluctance Actuator Gap Disturbance Testbed. The testbed emulates the short stroke and long stroke interaction of modern lithography stages. The testbed can be used to impart gap disturbance of the order of  $10\mu\text{m}$  to a target platten thereby providing a gap disturbance to the reluctance actuator. The testbed is equipped with three single-axis load cells that can measure a normal force, a roll torque and a pitch torque. We keep track of the orientation and position of the stage by using capacitance probes. The gap disturbance is imparted with three piezos capable of a stroke of  $15\mu\text{m}$ . We have also fabricated several reluctance actuators that fit into this testbed. These actuators use a two coil winding per core to prevent leakage and reduce stray torques. The cores of these actuators are made of Cobalt Iron, the soft magnetic material with the highest flux density saturation. Both a single actuator and a double actuator were fabricated. The double actuator can impart a roll torque as well as a normal force. Finite Element Method was utilized to design the actuators and to understand the nature of the rotational stiffness of the actuator. Experiments to do disturbance rejection were carried out and also different methods of force control (like Flux Feedback) are discussed and implemented.

Thesis Supervisor: David L. Trumper  
Title: Professor of Mechanical Engineering





## Acknowledgments

Graduate School is definitely the hardest thing I have done so far in my short career. I have many people to thank for helping me through these last two years. First I'd like to thank my advisor Prof. Trumper for letting me work in the Precision Motion Control Lab. I learned a ton of engineering and life lessons from him and I appreciate the patience and enthusiasm in his advising. Second, I'd like to thank my "other" advisor Ian MacKenzie, he introduced me to reluctance actuators and was always ready to help my research with his valuable insight. This thesis would not be possible without him.

Thank you to ASML for sponsoring my project, many thanks to Mark Schuster, Chris Ward and Steve Roux for their valuable feedback while on this project.

My labmates at PMC over the last two years have made graduate school an enjoyable experience. In a lab with no windows they were always the ones I turned to for some light and inspiration. Thanks to Darya, Jim, Mohammed, Ian, Minkyun, Joe, Jun-Young, Lei and Phillip for always making lab a friendly place to be in.

All the machining and fabrication for this thesis was done in the Laboratory for Manufacturing and Productivity, thanks to Pat McA., Dave D., Bill B., Dave L. and Gerry W. for all their help in getting my project finished. Many thanks to my friends at the Edgerton Center that helped me stay motivated and focused. Thanks to Alban, Sandi, Bob, Amy, Jess, Kim, Tony, Jim and Ed for always making me feel welcome at their workplace. I feel thrilled and privileged to be able to continue my professional career as an instructor in the Edgerton Center family. Thanks to the MIT Electric Vehicle Team for always being ready to provide me with a healthy distraction when I needed one, special thanks to Lennon Rodgers for igniting my passion for EVs. Thanks to Javier Ramos for being an awesome roommate who was always able to put things in perspective. Thank you to the entire N52/51 Community, including the clubs and teams, D-Lab and MITERS. Thanks to Dr. Araceli Isenia and Dr. Simon Lejeune at MIT Medical for literally keeping me sane for my last months of graduate school. Many thanks to Dana Braff and her puppy Scout for always being there for

me when I most needed it.

Last I'd like to thank my family for their support throughout the years and all their hard work that helped me attend and succeed at MIT. Muchas gracias Mami, Papi, Fer, Alvaro, Tita y Abuelita Lolita por su apoyo a través de los 24 años de mi vida, nada de esto fuera posible sin su cariño y fuerza. Gracias a mi tío José ya que a través de él fue quien primero descubrí las maravillas de la profesión de ingeniería. Esta tesis va dedicada a mis abuelitos Chitin, Olga y Juan "Daddy" [que en paz descansen]. Por último muchas gracias a Dios por todo lo que nos ha dado.

# Contents

<b>1</b>	<b>Introduction</b>	<b>15</b>
1.1	Key Results . . . . .	16
1.2	Layout of this Thesis . . . . .	16
<b>2</b>	<b>Background</b>	<b>21</b>
2.1	Photolithography Stages . . . . .	21
2.2	Motors used in Lithography Positioning . . . . .	25
2.2.1	Lorentz Motors . . . . .	25
2.2.2	Reluctance Actuators . . . . .	26
2.3	Conclusions . . . . .	29
<b>3</b>	<b>Reluctance Actuators: Modeling, Fabrication and Control</b>	<b>31</b>
3.1	Reluctance Actuator Modeling . . . . .	31
3.1.1	Stray Torques in Reluctance Actuators . . . . .	32
3.2	Fabrication of Reluctance Actuators . . . . .	34
3.2.1	Core Material . . . . .	35
3.2.2	Manufacturing . . . . .	36
3.3	Control of Reluctance Actuators . . . . .	39
3.3.1	Flux Feedback control of Actuator . . . . .	40
<b>4</b>	<b>Hardware</b>	<b>45</b>
4.1	Poovey Test Fixture . . . . .	45
4.2	Modifications to Test Fixture . . . . .	47

4.2.1	Piezo Actuators . . . . .	49
4.2.2	Instrumentation . . . . .	51
4.2.3	Control Software . . . . .	55
<b>5</b>	<b>Experimental Results</b>	<b>57</b>
5.1	Driving the Piezos . . . . .	57
5.2	Calibration of Actuators . . . . .	57
5.3	Disturbance Rejection via Feedforward . . . . .	60
5.4	Flux Feedback . . . . .	63
<b>6</b>	<b>Conclusion and Future Work</b>	<b>65</b>
6.1	Summary of Work . . . . .	65
6.2	Suggestions for Further Research . . . . .	65

# List of Figures

1-1	Gap Disturbance Testbed . . . . .	17
1-2	Position Disturbances on the Stage due to Piezo excitation at different voltages. . . . .	18
1-3	Single U-Core Actuator. . . . .	18
1-4	Double Core actuator can control force and torque. . . . .	19
2-1	Lithography tool manufactured by ASML. . . . .	22
2-2	Schematic of Lithography Process. . . . .	22
2-3	Short Stroke and Long Stroke Stages. . . . .	23
2-4	Error in Variable H (distance between LS and SS) as might be typical in a real lithography machine. . . . .	24
2-5	Lorentz Force Principle. . . . .	25
2-6	Cross Section of Typical Lorentz Actuator . . . . .	26
2-7	Basic Reluctance Actuator with an Amperian Loop to calculate the force-current characteristics. . . . .	27
2-8	Using the Maxwell stress tensor to calculate reluctance force. . . . .	28
2-9	An example of a single DOF short-stroke stage driven by reluctance actuators . . . . .	29
3-1	FEMM Flux Density Plot of E Shaped Reluctance Actuator . . . . .	32
3-2	E Shaped Reluctance actuator with a single winding in the center pole	33
3-3	E Shaped Reluctance actuator under angular disturbance . . . . .	33
3-4	U Shaped Reluctance actuator with two windings . . . . .	34
3-5	Flux Density along face of target in U actuator for 1 degree tilt . . .	35

3-6	Flux Density along face of target in E actuator for 1 degree tilt . . .	35
3-7	Typical Magnetic Hysteresis Loops . . . . .	36
3-8	Chart Showing maximum flux density vs Coercivity [taken from [?]] .	37
3-9	Completed Actuator . . . . .	37
3-10	Image of Fixture Plate for a two core actuator . . . . .	38
3-11	Cross Section of Potting Process . . . . .	39
3-12	Actuator left to dry overnight, note the permanent magnets used to hold cores in place. . . . .	40
3-13	Finished Double Actuator . . . . .	40
3-14	Feedback Linearization of Magnetic Suspension (taken from [8]) . . .	41
3-15	Reluctance Actuator with Hall Effect Sensor . . . . .	42
3-16	Reluctance Actuator with Sense Coil . . . . .	42
3-17	Flux Feedback Configuration . . . . .	43
3-18	Flux estimation and control using lookup tables (LUT) and comple- mentary filters (from [3]) . . . . .	43
4-1	CAD Drawing of the Poovey Test Fixture (taken from [6]) . . . . .	46
4-2	Force Plots for various gaps taken on Poovey fixture (taken from [6])	47
4-3	Gap Disturbance Testbed . . . . .	48
4-4	Cross section of Testbed with modifications . . . . .	49
4-5	Piezos Available from PI (taken from physikinstrumente.com) . . . .	50
4-6	Evaluation Kit for DRV8662 Amplifier (image taken from Texas In- struments) . . . . .	51
4-7	Circuit Layout for the DRV8662 Evaluation Board. Capacitors C4 and C5 were shorted out to allow for the amplifiers to output positive DC components . . . . .	52
4-8	Broken Piezo, notice the stack has completely sheared . . . . .	52
4-9	Two styles of mounting piezo adapter, notice the small gap on the right image allows for a thin wrench to be inserted when unscrewing the piezo	53

4-10 Hexagonal Arrangement of cap probes and kinematic mounts on target platten . . . . .	54
4-11 Coordinates with respect to reluctance actuator . . . . .	54
4-12 Geometry of Load Cell Positions . . . . .	55
5-1 Stage response to Piezos at different voltage amplitudes. . . . .	58
5-2 Disturbance in the force do to a 5 micron disturbance at 300 micron nominal gap (constant 1A current) . . . . .	59
5-3 Cobalt Actuator (left) Nickel Actuator (right) . . . . .	60
5-4 Dynamic signal analysis to determine cobalt actuator parameters at 300 $\mu$ m. . . . .	61
5-5 Compensated loop for the current controller in Cobalt Actuator. . . . .	61
5-6 Force vs Current at different gaps for Nickel Actuator, notice the hysteresis and the saturation apparent in the 100 micron curve. . . . .	62
5-7 Force vs Current profiles fitted with a quadratic model. . . . .	62
5-8 Feedforward control configuration. . . . .	63
5-9 Flux linkage vs current in cobalt actuator at 300 micron gap, notice the width of the loop due to ferromagnetic hysteresis in the cobalt . . . . .	64
5-10 Force vs. Flux linkage in cobalt actuator at 300 micron gap, notice the quadratic relationship and the lack of noticeable hysteresis . . . . .	64
6-1 When multiple actuators are used in a stage configuration, the parasitic effects need to be compensated using active control in all DOFs. . . . .	66
6-2 Reluctance Actuators are relatively compact to package in a stage, they can potentially be used for overactuation of a rigid body and dampen out the first couple of flexible modes for more complete control of the stage. . . . .	67
6-3 Package-less Hall Effect Sensors could lead to better flux sensing without too much air gap loss. . . . .	68
6-4 Deformation of stage when a 2 Amp peak sine wave is passed through the actuator. . . . .	68





## List of Tables



# Chapter 1

## Introduction

The photolithography industry has been growing for decades and enabling the creation of smaller faster and more reliable electronic components. In order to keep up with the increasing demand of performance and precision from the manufacturers and consumers, makers of photolithography equipment have to push the boundaries of their technologies to achieve the specs of precision and speed that are required.

In photolithography, the precision and speed of positioning stages are of utmost importance. Given the wafers must go in and out of the machine several times during the manufacturing process the machine must be able to locate each wafer to high degrees of accuracy and repeatability. In addition the positioning must be done fast, the faster the actuators can move the stage the more wafers per hour the machine can produce. The motors used in driving the stages are a key part in giving the system reliability and speed. Historically, the photolithography industry has used Lorentz actuators on their stages. Lorentz actuators employ a coil of wire and a permanent magnet which results in force production that is highly linear and non-stiff. An alternative to Lorentz actuators is Magnetic Reluctance Actuators, these work based on the purely attractive reluctance force between a magnetized core and a ferromagnetic target. Reluctance actuators are hysteretic, non-linear and stiff which makes them hard to control, however the force density (amount of force per unit of moving mass) of these actuators is superior to the force densities of Lorentz actuators. As the photolithography industry pushes for higher forces and accelerations reluctance

actuators are an attractive alternative to the motors of today.

## 1.1 Key Results

As part of this research we have designed and built a testbed to test gap disturbance rejection in reluctance actuators. We took an existing fixture for calibrating magnetic bearings built by Poovey in [6] and modified it to make gap disturbance tests. We relocated the load cells and added piezoelectric actuators to provide the disturbance on the target platen. The hardware is shown in fig 1-1. This new hardware can now be used to impart gap disturbances (of the same nature that exist in a lithography stage system) and test out ways of rejecting them with a control system.

Fig 1-2 shows a plot of the stage position under excitation by the piezos. The excitation frequency and amplitude are representative of gap disturbances encountered in real lithography stages.

As part of the study, several reluctance actuators were produced. These actuators use Cobalt Iron (also known as Supermendur) as their core material. Cobalt Iron has the highest magnetic saturation of any readily available soft magnetic metals. This high saturation limit allows for greater force densities of the actuator. The actuators were wound, machined and potted by the author, a single core actuator is shown in fig 1-3. A double core actuator was also fabricated, this actuator has two separately excited coils and can generate a roll torque as well as a normal force. A picture of this actuator is shown in Fig 1-4. More details on the reluctance actuators manufactured are presented in chapter 3.

## 1.2 Layout of this Thesis

We introduced the work by talking about its nature and motivations in this chapter. Chapter 2 gives background information on Reluctance and Lorentz motors and their use in photolithography stages. Chapter 3 talks about magnetic modeling of reluctance actuators and their design. Chapter 4 talks about the hardware that was

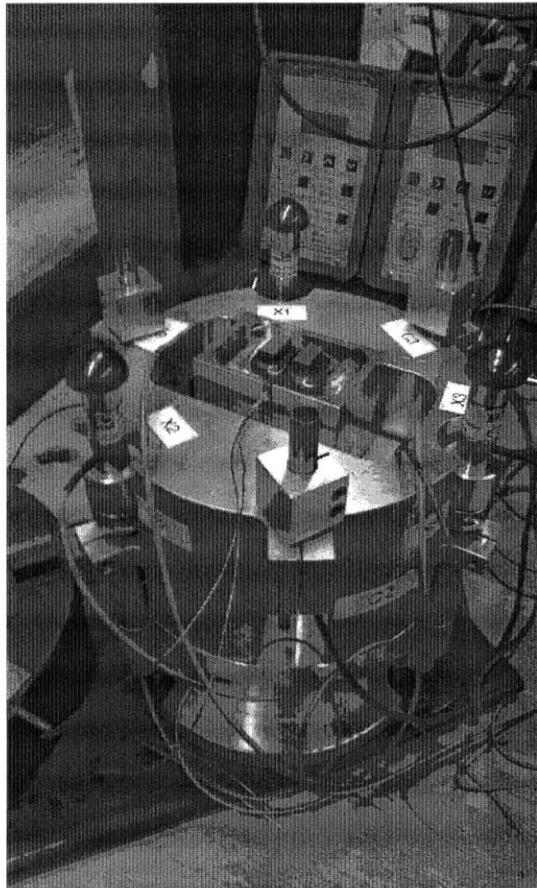


Figure 1-1: Gap Disturbance Testbed

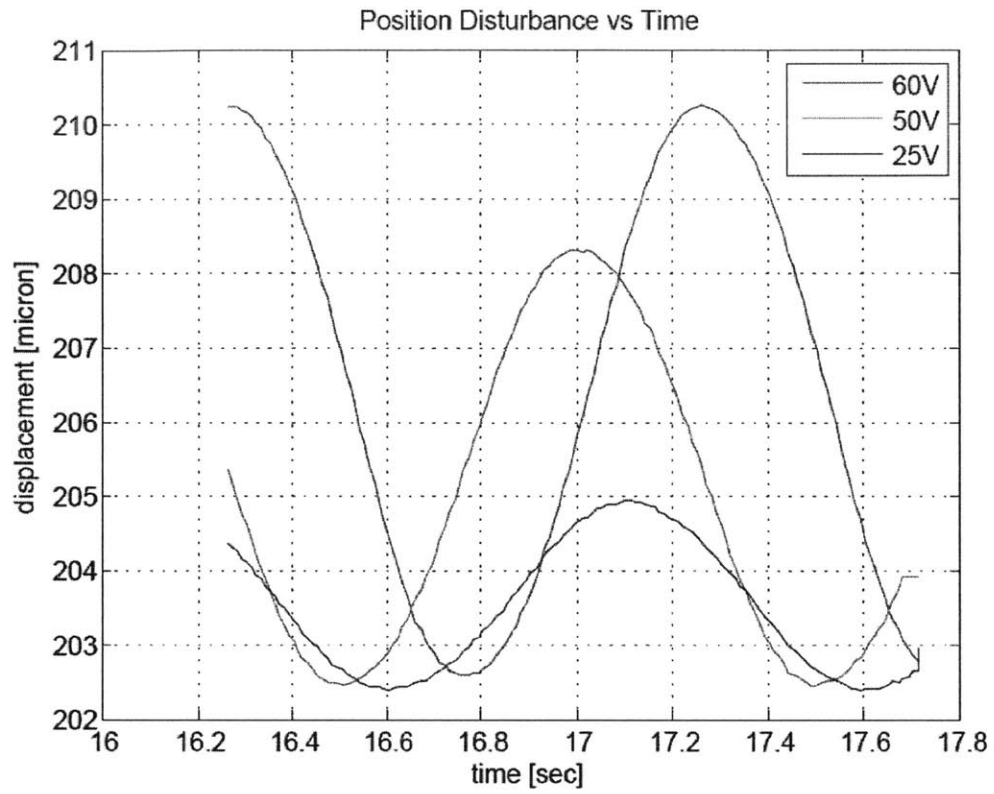


Figure 1-2: Position Disturbances on the Stage due to Piezo excitation at different voltages.



Figure 1-3: Single U-Core Actuator.

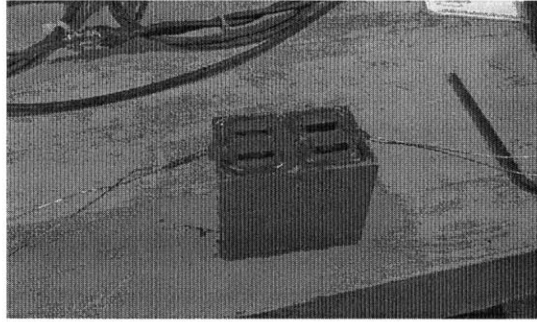


Figure 1-4: Double Core actuator can control force and torque.

designed and fabricated for this research. Chapter 5 presents experiments and results using the hardware. Chapter 6 summarizes the work and suggests directions for further research.





# Chapter 2

## Background

This chapter provides a brief introduction to photolithography stages and talks about the basic configurations of reluctance and Lorentz linear motors. We derive the basic calculations commonly used when dealing with these two types of motors. In addition we also discuss the issue of stiffness in the actuators and why its problematic. For a more complete overview of positioning in lithography tools see Hans Butler's discussion in [1].

### 2.1 Photolithography Stages

Integrated Circuits (ICs) are produced by a manufacturing process in which a silicon wafer acts as a base and then semiconductor structures are built layer by layer on it. This manufacturing technique is known as photolithography. This process lays down patterns of chemicals that form the transistors and other circuit elements that form part of the final product. The patterns get transferred to the wafer via an "optical stencil" known as the mask or the "reticle". Photolithography tools (produced by companies like ASML and Nikon) shine light through the reticle onto the wafer to form the 2D patterns required by the designers of ICs. After exposure the wafer exits the machine and is then subjected to one or many chemical processes to etch the desired pattern. After some time the same wafer will re-enter a photolithography tool (not necessarily the same one) and another pattern will be exposed on it. Repeatability

is extremely important given all the 2-dimensional layers in the structure form a 3-dimensional structure and if layers are misaligned over the tolerance then the chip will not function as designed. Also, as in every manufacturing process we want the tool to function as quickly as possible in order to produce most wafers per hour possible.

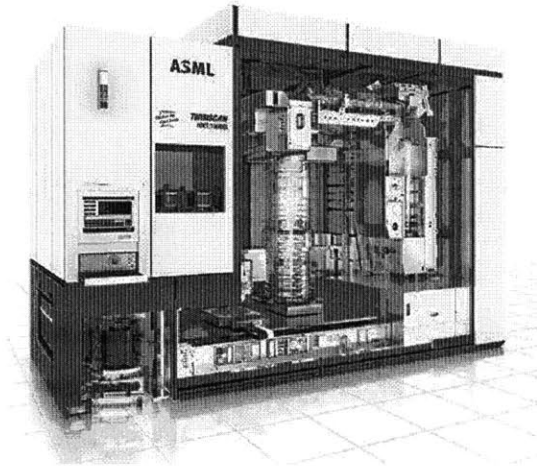


Figure 2-1: Lithography tool manufactured by ASML.

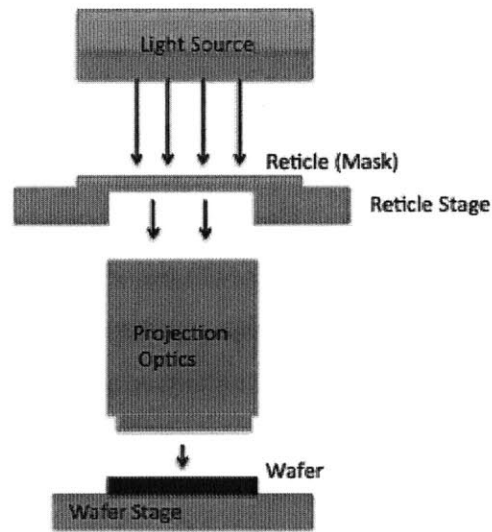


Figure 2-2: Schematic of Lithography Process.

The lithography tool has both a reticle stage and a wafer stage. In between the two stages there are a number of projection optic elements that reduce the size of

the optical features by some scale (typically 4:1 reduction). Both the wafer and reticle stages move in opposite directions under the scan process. Because of the projection optics the reticle stage must move 4 times faster than the wafer stage. The accelerations involved in these processes are of the order or 16g and the industry is pushing for them to increase.

An industry standard wafer size is 300mm, this sets the minimum for the travel of the wafer stage. The reticle stage must have a travel of 4 times the field size of the wafer. State of the art lithography tools have reticle stage travel range on the order of a couple of 400mm and they must be accurate to nanometers. A sensor with range of meters and resolution of nanometers is simply not available anywhere at this point in time. Thus what is typically employed in a commercial system is a two part stage, one part being the coarse stage (also called the Long Stroke, LS) and the other being a fine stage (called the Short Stroke, SS). The LS has meter range and micron accuracy, whereas the SS has micron range but nanometer accuracy. The LS positions the stage within microns of the desired set point and then the SS (which rides on the LS) positions the stage to nanometer accuracy.

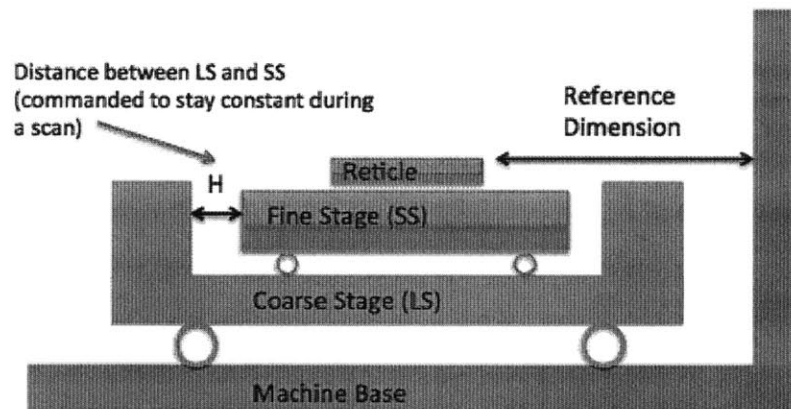


Figure 2-3: Short Stroke and Long Stroke Stages.

Under closed loop the stages work together to move the reticle (which rests on the SS), as depicted in Fig.2-3. Their control loops are decoupled. The SS is given a reference trajectory while the LS tries to keep the gap between the SS and LS

constant. A typical error in this variable H is shown in the plot in Fig. 2-4. Similar control schemes are used in the other degrees of freedom. The actuators and control system must be able to reject this “gap disturbance” to achieve position accuracy. This is where the stiffness of the actuator becomes important.

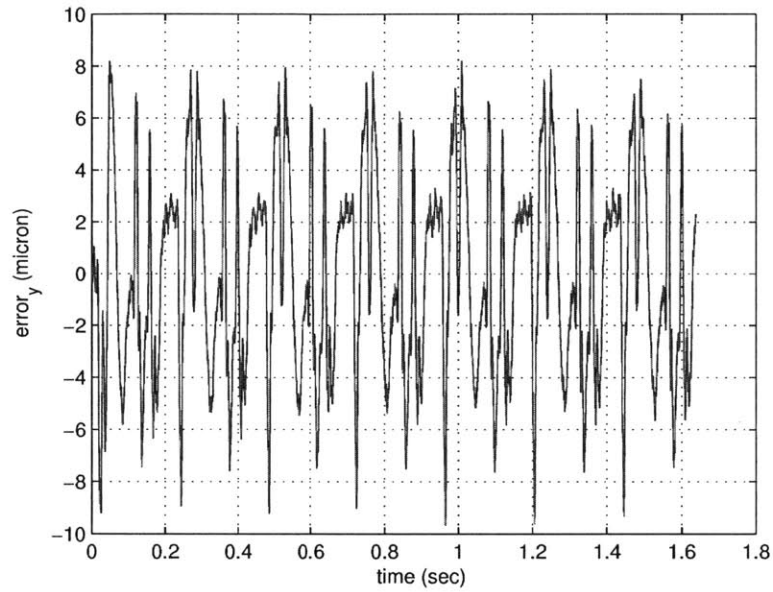


Figure 2-4: Error in Variable H (distance between LS and SS) as might be typical in a real lithography machine.

## 2.2 Motors used in Lithography Positioning

### 2.2.1 Lorentz Motors

Currently most motors used in photolithography stages are Lorentz-type motors. These electromagnetic actuators provide a repeatable force without any contact or friction. The simplest of Lorentz motors consist of two main parts, a pair of permanent magnets and a coil of wire. In the area between the magnets a magnetic field  $B$  is established and when current  $i$  flows through the wire a force is produced that is equal to  $il \times B$ , where  $l$  is the length of wire in the field  $B$ . A simplified schematic of the Lorentz force is shown in Fig. 2-5.

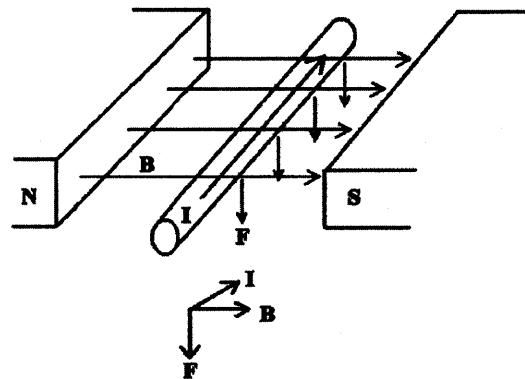


Figure 2-5: Lorentz Force Principle.

Assuming the magnetic field is roughly constant in the travel of the actuator, (a reasonable assumption given quality magnets and appropriate coil magnet spacing) the force produced is not dependent on position or travel of the stage. Thus the actuator is said to not be stiff. Fig 2-6 shows the cross section of a typical Lorentz motor. In this actuator the force is given by: (Here  $D$  is the Depth,  $N$  is the number of turns,  $B$  the Magnetic Field Density and  $i$  the current in the wire.)

$$F = 2BiDN \quad (2.1)$$

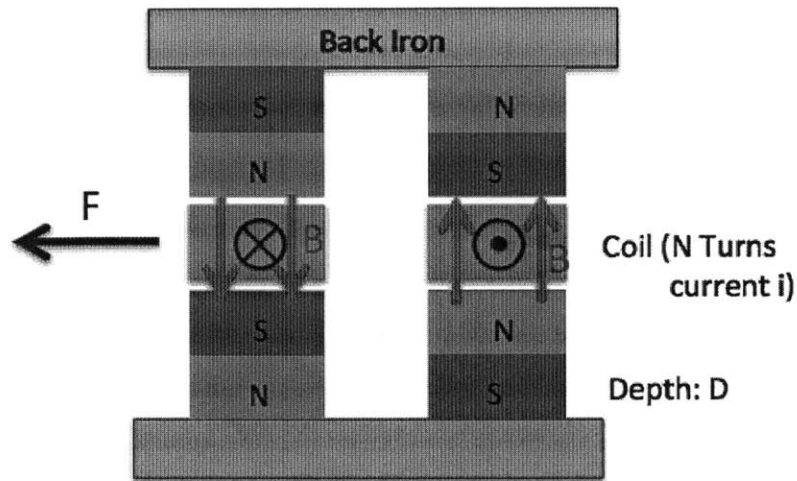


Figure 2-6: Cross Section of Typical Lorentz Actuator

### 2.2.2 Reluctance Actuators

Reluctance Actuators work on the principle of reducing the reluctance of a magnetic circuit. An example of reluctance force is the interaction between an electromagnet and a piece of steel. The force is always attractive and also position dependent (i.e. stiff). Fig. 2-7 shows a basic configuration for a reluctance actuator. Similar to the Lorentz actuator it contains a coil winding but it doesn't necessarily have to contain a permanent magnet. When the coil is energized, a magnetic circuit is established. The amount of attractive force can be estimated using ampere's law and the Maxwell stress tensor, as described below.

Ampere's Law states that the line integral of the magnetic field over a closed contour is equal to the surface integral of the current density penetrating that contour. Using this law we can calculate the Magnetic Flux density in the gap  $B_g$ .

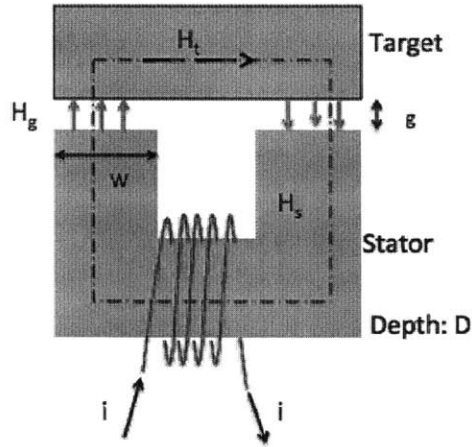


Figure 2-7: Basic Reluctance Actuator with an Amperian Loop to calculate the force-current characteristics.

$$\oint_C H \cdot dl = \oint_s J \cdot dA$$

$$2gH_g + l_t H_t + l_s H_s = Ni \quad H_g \gg H_t, H_s$$

$$H_g \approx \frac{Ni}{2g}$$

$$B_g \approx \frac{Ni}{2g} \mu_o$$

With  $B_g$ , the Maxwell stress tensor can now be used to calculate the reluctance force. Fig 2-8 shows the surface used in the stress tensor to calculate the force on the target plate. We are ignoring leakage flux in this example, thus the only surface that will contribute to the maxwell stress tensor is side 4.

Assuming a constant permeability  $\mu$  and ignoring magnetostriction, the elements of the Maxwell stress tensor are given by: [5]

$$T_{ij} = \mu H_i H_j - \frac{1}{2} \delta_{ij} \mu H^2 \quad (2.2)$$

$$T_{xx} = \frac{1}{2} \mu H_x^2 \quad (2.3)$$

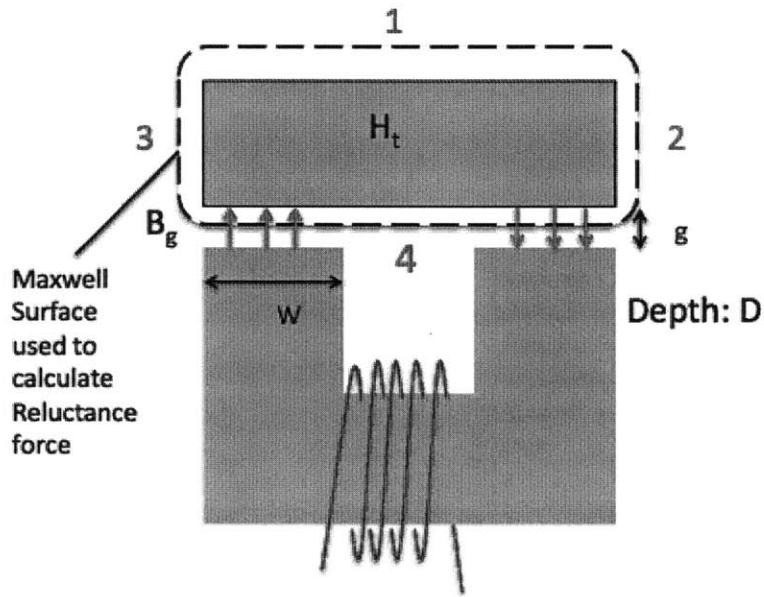


Figure 2-8: Using the Maxwell stress tensor to calculate reluctance force.

The force is evaluated by integrating the Stress Tensor over an Area. By assuming constant fields in the gap and an Area  $A = WD$  for our example we obtain the following:

$$F = \oint T_{xx} dA \quad (2.4)$$

$$F = T_{xx} A \quad (2.5)$$

$$F = A \frac{1}{2} \mu H_x^2 = \frac{1}{2} \mu \frac{B_g A}{\mu_0} \quad (2.6)$$

Plugging in for our particular geometry gives the following result

$$F = 2WD \frac{1}{2} \mu \frac{N^2 i^2}{4g^2} \quad (2.7)$$

In the previous analysis we assumed an  $H$  of zero in the ferromagnetic core and target. Thus we were able to arrive at a simple expression of the force. In reality



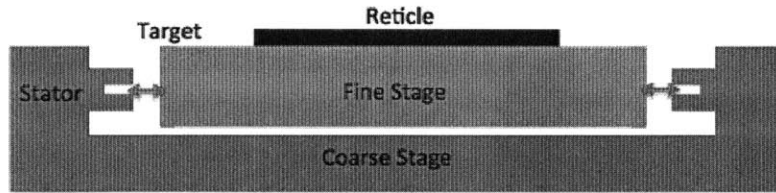


Figure 2-9: An example of a single DOF short-stroke stage driven by reluctance actuators

however the  $H$  in the core is not zero, and it factors into amperes law thus degrading the amount of force the actuator creates. Furthermore, in the core the mapping from  $B$  to  $H$  is not one to one. That transformation is hysteretic which means the force will not be repeatable. Formulating an accurate hysteresis model and using it in real time is important to achieve accurate control of the force in reluctance actuators . For further information I recommend references [3] and [2] both which provide good analysis and modeling of ferromagnetic hysteresis and its role in reluctance actuators.

Given the reluctance force is only attractive, there need to be two actuators per bidirectional degree of freedom on a stage. An example of a stage concept controlled in one axis with reluctance actuators is shown in Fig. 2-9.

## 2.3 Conclusions

The actuator comparison shows that the fundamental tradeoff between Lorentz actuators and Reluctance Actuators is performance potential vs controllability of the actuator. Reluctance Actuators provide better performance in terms of theoretically achievable accelerations and power dissipation, however their non-linearities make them harder to control to the desired specs by the lithography industry. As the industry moves forward engineers are going to have to devise ways to control reluctance actuators more accurately to keep with the growing performance demands of customers. An industry comparison of both actuators is given in [7].



## Chapter 3

# Reluctance Actuators: Modeling, Fabrication and Control

This section focuses on reluctance actuator modeling, design and control. We extend the simple reluctance model of Chapter 2 by using Finite Element (FE) tools. The finite element tools are also used to characterize the stray torques and torsional stiffness of the actuators. Different actuator configurations are introduced and their advantages and disadvantages are presented. Manufacturing tips for reluctance actuators are also presented. Finally, different forms of control of reluctance actuators are presented and explained.

### 3.1 Reluctance Actuator Modeling

The model presented in Chapter 2 accounts for the basic behavior of reluctance actuators. This model however does not take into account important non-idealities such as hysteresis, saturation and fringing fields. Finite Element Analysis (FEA) is used to better model these actuators. For this study FEMM (Finite Element Method Magnetics), an open-source 2-D FEA program is used [4]. FEMM can deal with non-linearities such as saturation and fringing fields, unfortunately as far as the author is aware no FE package at this moment can effectively deal with magnetic hysteresis.

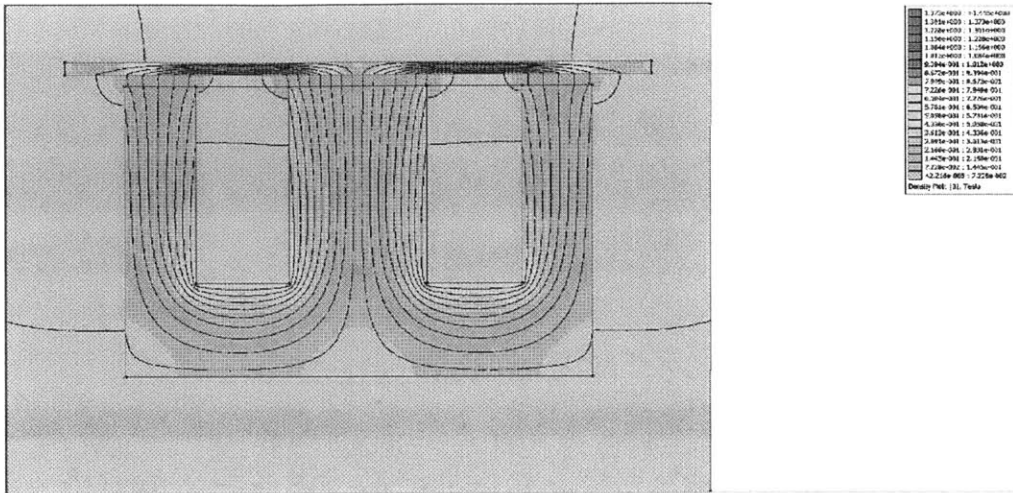


Figure 3-1: FEMM Flux Density Plot of E Shaped Reluctance Actuator

### 3.1.1 Stray Torques in Reluctance Actuators

Reluctance motors are a source not only of force but also of unwanted (stray) moments. These moments come about when the stator and target faces are not parallel to each other. These moments can cause errors in the stages and cause the actuator to have an undesired torsional stiffness.

These moments come about because of the non-symmetrical distribution of the magnetic flux density. The amount of stray torque is highly dependent on the type of magnetic circuit that is used. Consider the magnetic configuration shown in fig 3-2 with an “E” shaped actuator. This configuration has three gaps between the stator and target. When the target rotates relative to the stator the path length of one of the sides shortens which causes a drop in reluctance and thus higher flux density  $B$  in that gap, see Fig. 3-3 . This configuration with multiple paths for the flux is very prone to stray torques.

Another commonly used configuration is shown in Fig. 3-4. This configuration (using a “C” shaped actuator) only has one path for the magnetic flux to flow. This forces the Flux density to be essentially constant as long as the cross section area remains roughly constant. This configuration also shows two coils per core, the coils are oriented such that one of the coils pushes flux into the target and the other one

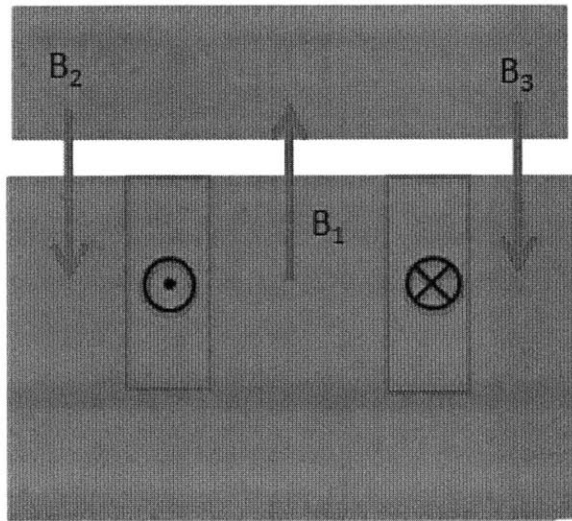


Figure 3-2: E Shaped Reluctance actuator with a single winding in the center pole

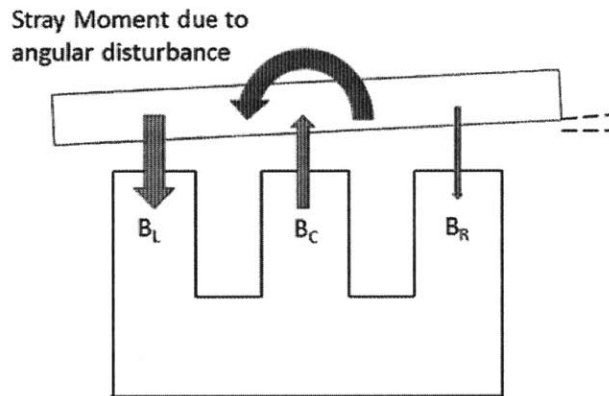


Figure 3-3: E Shaped Reluctance actuator under angular disturbance

“pulls” flux from the target. Using one coil as a “source” and the other as a “sink” of magnetic flux for the target provides a more clearly defined magnetic circuit and minimizes leakage flux.

The U actuator is less torsionally stiff in the magnetic sense than its E shaped counterpart. This minimizes the stray torques from actuators with this configuration. However these actuators will still exhibit stray torques, Fig. 3-5 shows the magnetic flux density along the face of the ferromagnetic target in a U actuator. The asym-

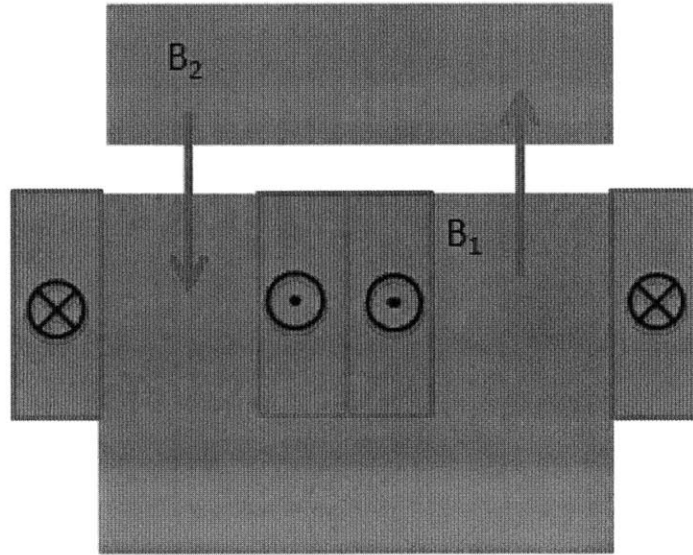


Figure 3-4: U Shaped Reluctance actuator with two windings

metric flux distribution indicates that a stray torque will be created. For comparison Fig. 3-6 shows the flux distribution on the E shaped actuator of a similar size. From comparing the flux along the target face for these two cases it becomes apparent that the E actuator will have a higher rotational stiffness given the asymmetry in the graph.

## 3.2 Fabrication of Reluctance Actuators

As part of this work several actuators were fabricated. The actuators were built using cobalt-iron cores (this material is known as Supermendur in industry). These cores offer the highest magnetic saturation of soft magnetic metals. Such high saturation is desirable because the maximum force is limited by the square of the maximum magnetic flux that the material can carry.

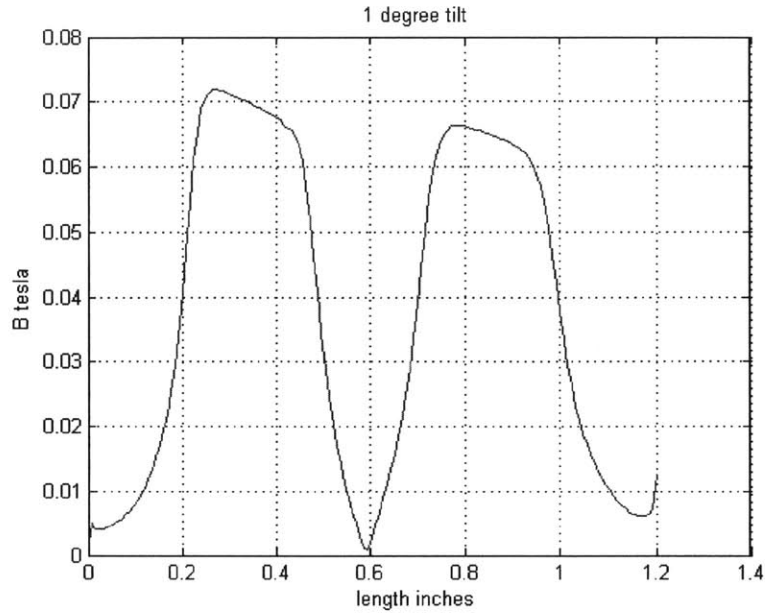


Figure 3-5: Flux Density along face of target in U actuator for 1 degree tilt

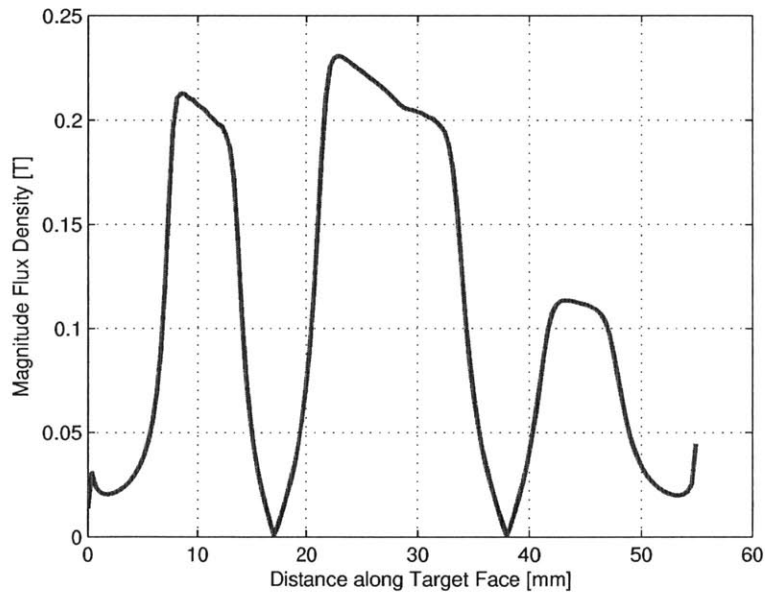


Figure 3-6: Flux Density along face of target in E actuator for 1 degree tilt

### 3.2.1 Core Material

The magnetic core material plays an important part in the performance of the reluctance actuator. The amount of flux that can be sustained by the core (its magnetic

saturation) puts a limit on the amount of force that can be produced by a certain actuator. The core's magnetic hysteresis is another factor that affects the performance of the actuator. When selecting a core material there is often a tradeoff between the coercivity (proportional to hysteresis) and flux saturation (which defines maximum force attainable). The perfect core for a reluctance actuator would have a high saturation limit and very low coercivity. However in reality this is not the case and often higher saturation materials also have a higher amount of coercivity. Fig. 3-7 shows typical hysteresis curves for a soft and a hard magnetic material. The wider the hysteresis loop the more hysteresis will contribute to force inaccuracies. Fig. 3-8 shows a chart of Saturation vs Coercivity for different soft magnetic materials. For our application we decided on Cobalt Iron cores given they have the magnetic highest saturation limits.

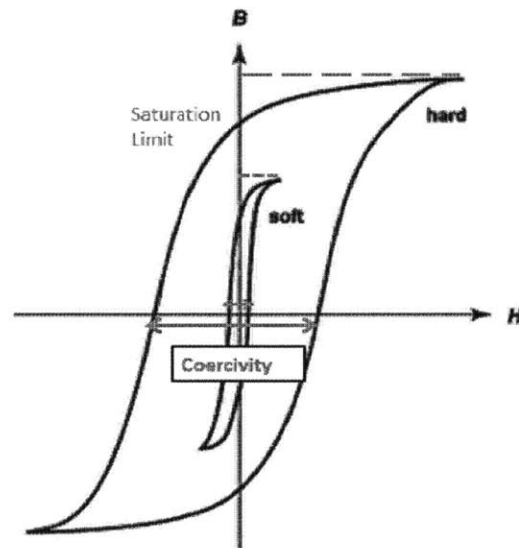


Figure 3-7: Typical Magnetic Hysteresis Loops

### 3.2.2 Manufacturing

As part of this work several actuators were produced. The winding, machining and potting of the actuators were all done by the author. Fig 3-9 shows a picture of a completed actuator.



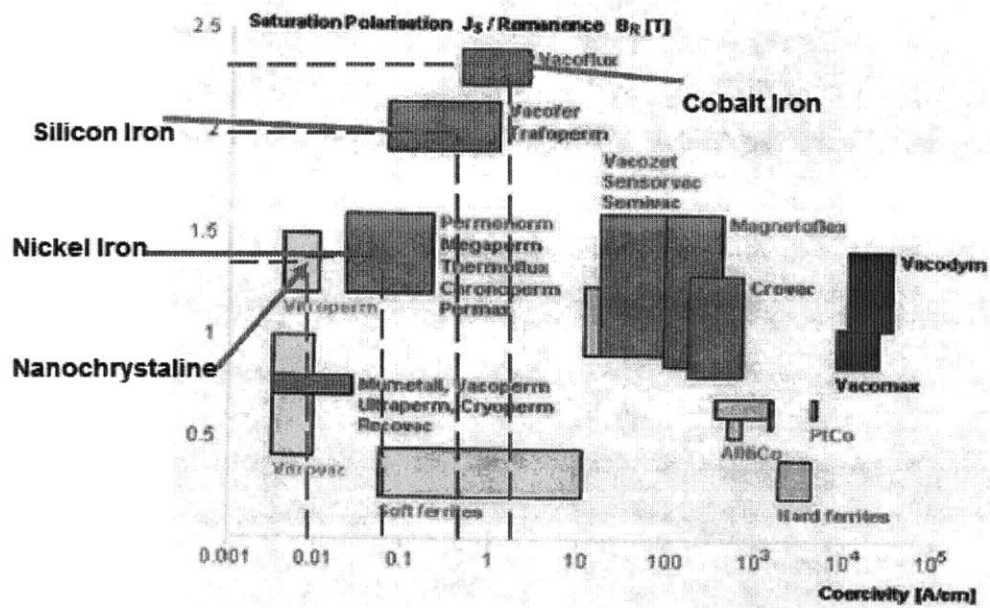


Figure 3-8: Chart Showing maximum flux density vs Coercivity [taken from [?]]



Figure 3-9: Completed Actuator

The U cores for the actuators were obtained from Magnetic Metals, these are Supermendur cores originally intended to be used as transformer cores. In order to wind these actuators a template was machined to wind the wire around and then transfer this to the U core. The mandrel (or template) is a piece of machined aluminum, to

wrap the magnetic wire around. The dimensions of the mandrel are 0.010 in bigger than the dimensions of the core, this ensures a good fit of the coil on the core. The mandrel is covered in kapton tape for insulation. The mandrel gets attached to the shaft of a geared universal motor that is controlled by a foot-pedal. The magnetic wire is fed by hand onto the mandrel. After every layer of winding epoxy is added to the winding. After the appropriate number of layers have been wound, the epoxy is left to dry overnight.

The housings are machined from aluminum and contain a cavity for the actuator and epoxy. Slots are machined on the sides of the housing for the wires to exit the assembly. When exiting the housing, wires must be insulated to prevent any potential shorts with the aluminum housing. An insulation multimeter (also called a megger) can be used to test the insulation of the core, housing and winding. A megger we used in this study can be found in [?]. Failure to have proper insulation of these components can lead to eddy currents and other non-ideal behaviors of the actuator.

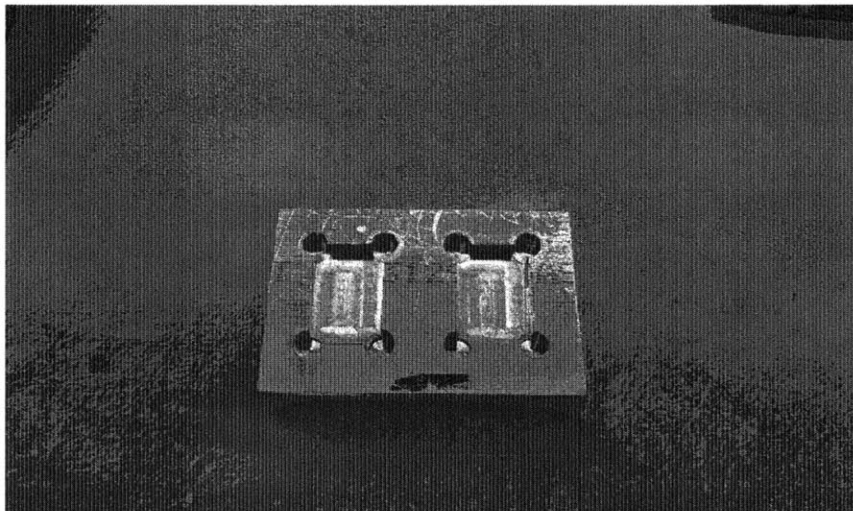


Figure 3-10: Image of Fixture Plate for a two core actuator

In order to pot the actuator accurately, a fixture plate was machined. The fixture plate shown in Fig. 3-10 has pockets milled on it that position the actuator in the housing. After the windings have been placed on the core the cores are placed in the fixture and held in place via a permanent magnet. This fixture-core assembly then

gets placed in the cavity which is half filled with epoxy. Gage blocks are placed to hold the housing and fixture in a fixed position see Fig 3-12. A cross section view of the potting setup is shown in 3-11 The whole assembly is left to cure overnight. The process is very similar for single and double actuators except the fixture plate is modified to accommodate two cores. A finished double actuator is shown in Fig 3-13. This double actuator can be used to create a roll torque on the platen.

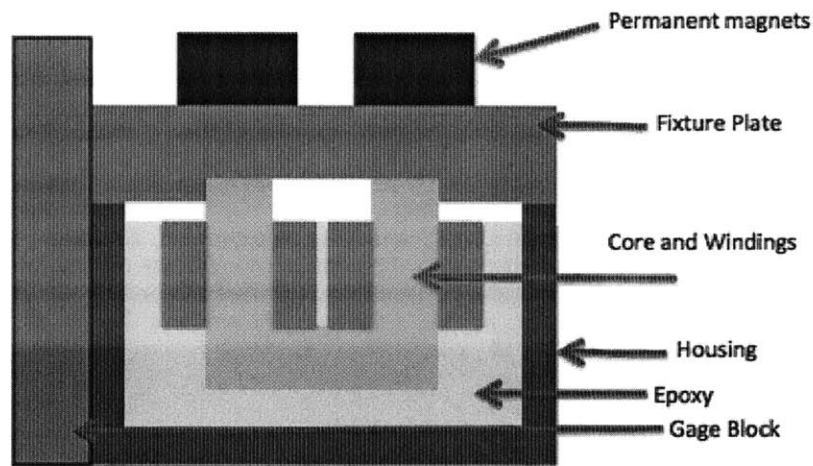


Figure 3-11: Cross Section of Potting Process

### 3.3 Control of Reluctance Actuators

Force control of reluctance actuators can be achieved in various ways. It is possible to create a linearized model for the actuator at a particular operating point. Such a method is used in [8]. This method gives acceptable results for gaps close to the linearizing point. Another way to control an actuator is via feedback linearization (also described in [8]). In this technique the position of the actuator is fed back to a non-linear compensator to attempt to eliminate the gap dependence of the actuator.

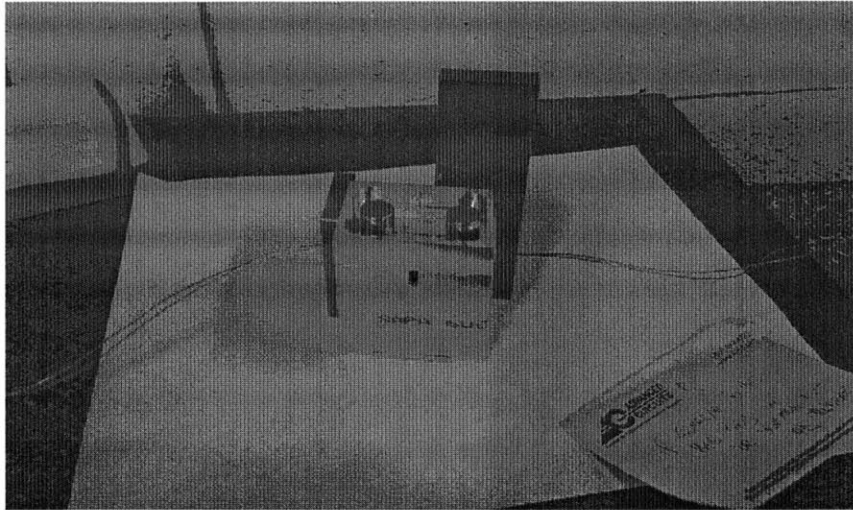


Figure 3-12: Actuator left to dry overnight, note the permanent magnets used to hold cores in place.

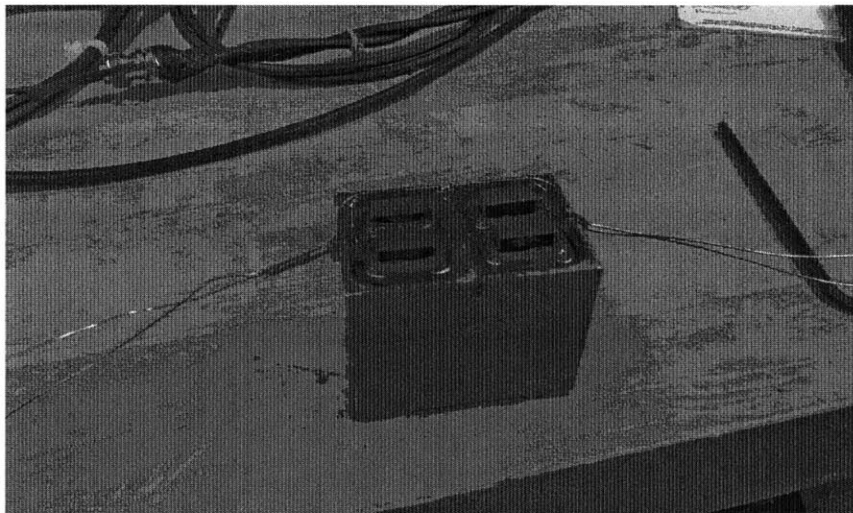


Figure 3-13: Finished Double Actuator

### 3.3.1 Flux Feedback control of Actuator

Both feedback linearization and operating point linearization depend heavily on having an accurate model for the actuator. Another method of control that depends less on an accurate model is flux control. Given the force delivered by a reluctance actuator is dependent of the square of the flux in the air gap, by monitoring and controlling the flux, the force can also be controlled.

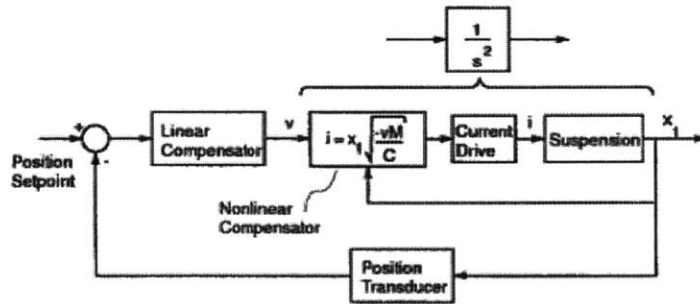


Figure 3-14: Feedback Linearization of Magnetic Suspension (taken from [8])

Measuring the flux is non-trivial, hall effect sensors provide a measurement of the flux in the air gap (see Fig. 3-15) however they are challenging to incorporate into an actuator given that they compromise the gap at which the actuators would operate. A sense coil can also be used to measure the flux in the air gap. The voltage generated in the sense coil is proportional to the rate of change of flux linked by the coil. This is shown in Fig. 3-16. The voltage can then be integrated to estimate the amount of flux in the air gap, and close a control loop on this variable. However, the sense coil does not provide true DC measurements of the flux. Thus for DC and low frequencies other control techniques need to be used to provide accurate forces. Fig. 3-17 shows a control configuration for force control using flux feedback.

In [3] the author shows a way to generate up an estimate of the flux in the gap by using lookup tables and a complementary filter pair. This approach uses the sense coil to estimate the high frequencies and it uses a lookup table between current and flux to estimate the low frequencies components of the flux. A schematic of this process is shown in 3-18.

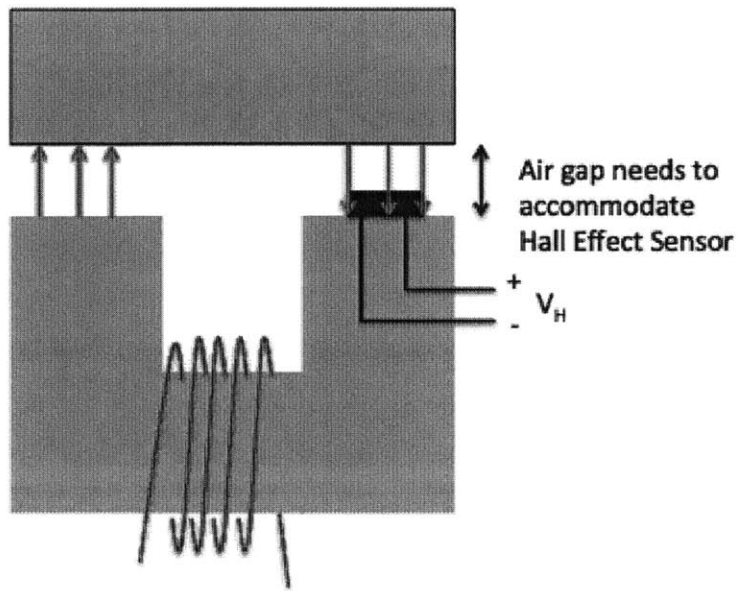


Figure 3-15: Reluctance Actuator with Hall Effect Sensor

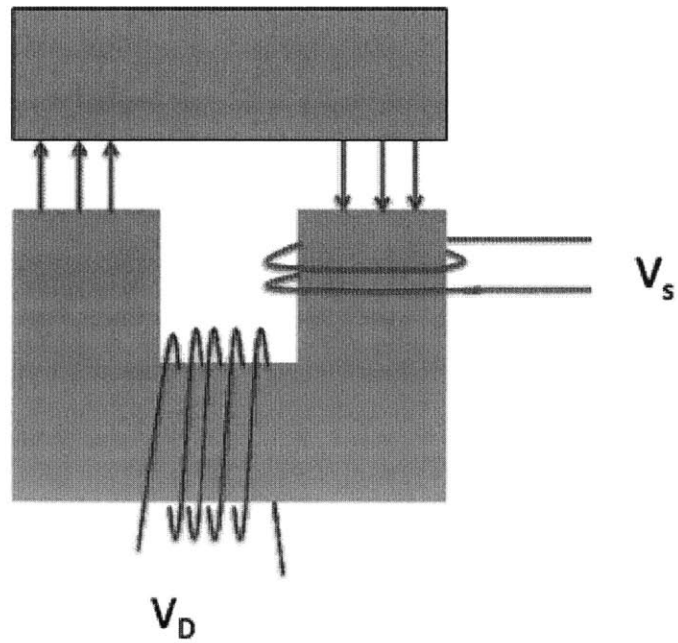


Figure 3-16: Reluctance Actuator with Sense Coil

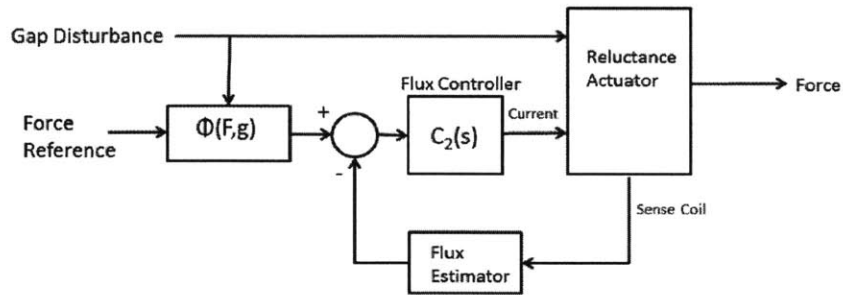


Figure 3-17: Flux Feedback Configuration

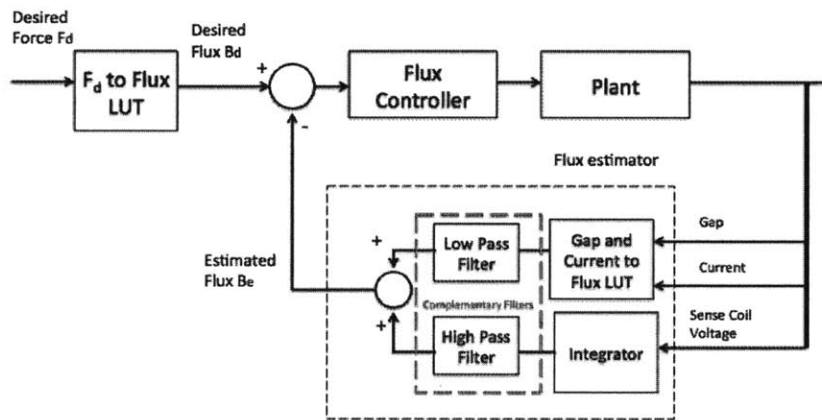


Figure 3-18: Flux estimation and control using lookup tables (LUT) and complementary filters (from [3])





# Chapter 4

## Hardware

This chapter describes the hardware that was designed and utilized for the experiments performed. This includes an intro to the Poovey test fixture described in [6] and the modifications made to it by the author. Elements of the power electronics and control software are also presented.

### 4.1 Poovey Test Fixture

In 1990 Poovey and Trumper fabricated a test fixture for reluctance actuators. The fixture is presented in [6]. This test fixture uses a silicon carbide kinematic coupling for repeatability and stiffness. The fixture utilizes piezo-electric load cells as the force sensors. Their high stiffness allows for accurate characterization of the actuators at frequencies below about 1kHz. Such high frequencies are not possible with other kinds of sensing elements like strain gauges, due to their relatively low stiffness. The fixture has 3 capacitance probes which can provide the 3DOFs of the target platen (z position, roll and pitch). Micrometers are used to set the nominal gap at which the actuator is tested. Fig. 4-1 shows a CAD drawing of the fixture as designed by Poovey. Fig 4-2 shows some data taken by the original fixture.

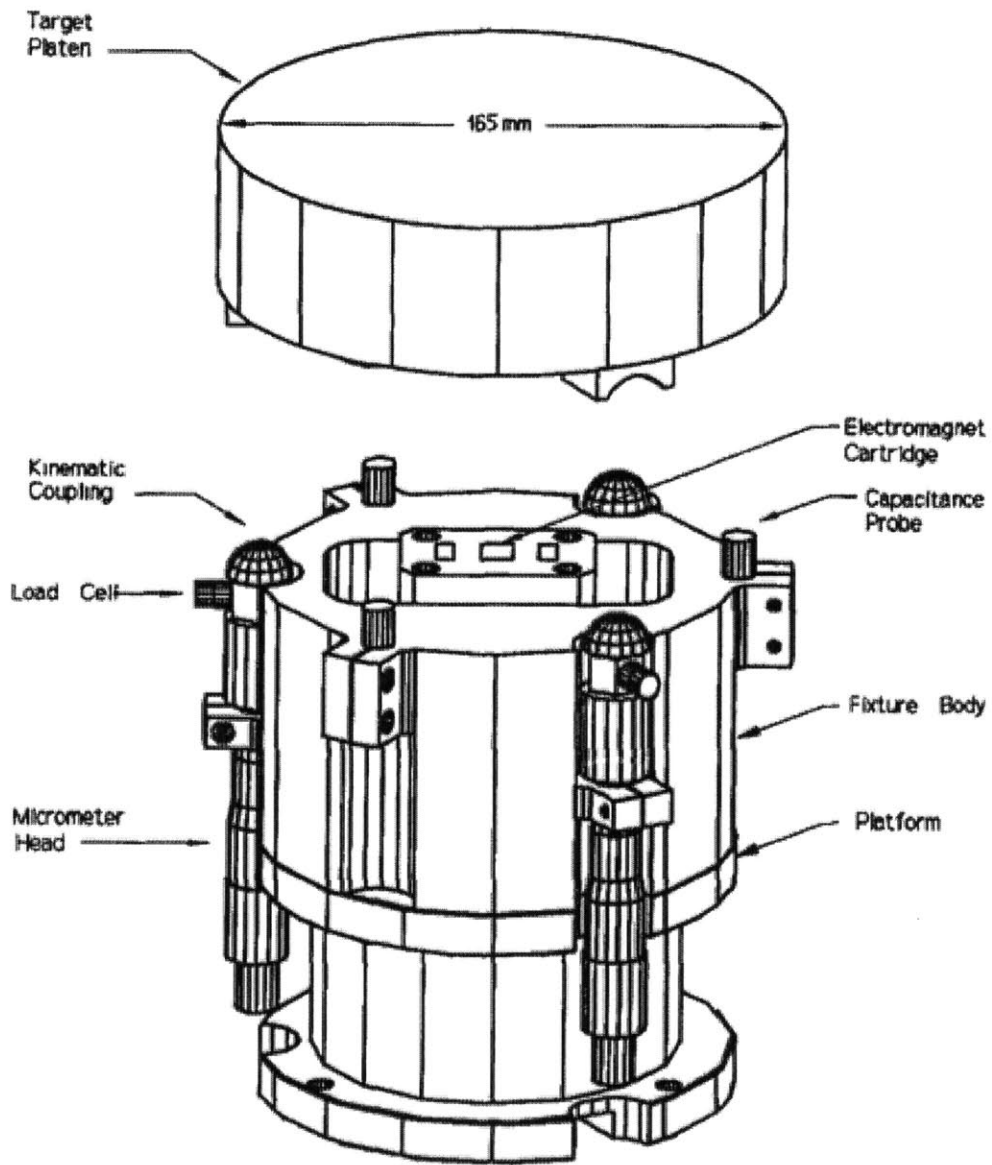


Figure 4-1: CAD Drawing of the Poovey Test Fixture (taken from [6])

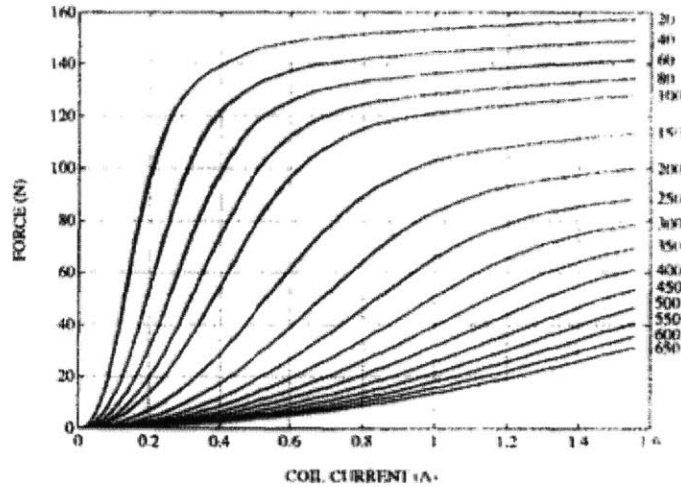


Figure 4-2: Force Plots for various gaps taken on Poovey fixture (taken from [6])

## 4.2 Modifications to Test Fixture

In the past the fixture was used to do tests with a gap, set by the micrometers. We modified the fixture to inject dynamic micron-scale disturbances in the gap. This provides an analog to the interaction between the short stroke and the long stroke stage in photolithographic equipment in which the suspension gap varies due to long-stroke vibrations.

Fig. 4-4 shows a cross section of the modified stage, while Fig. 4-3 shows a picture of the finished hardware. Piezo-electric actuators were added to actuate the platen in 3 degrees of freedom. The load cells were relocated to be static and inside the pocket of the fixture. Relocation of the load cells was necessary given they needed to be placed in the non-accelerating part of the fixture. Failure to relocate the load cells to a static location would make it impossible for the load cells to differentiate between acceleration and force signals.

The fixture still uses the micrometers to set a nominal gap (typically around  $300\mu\text{m}$ ) and it uses the piezos to provide disturbance around that gap. Capacitance probes feed the position information in real time to the controller, which tries to follow a force profile in the face of the disturbance.

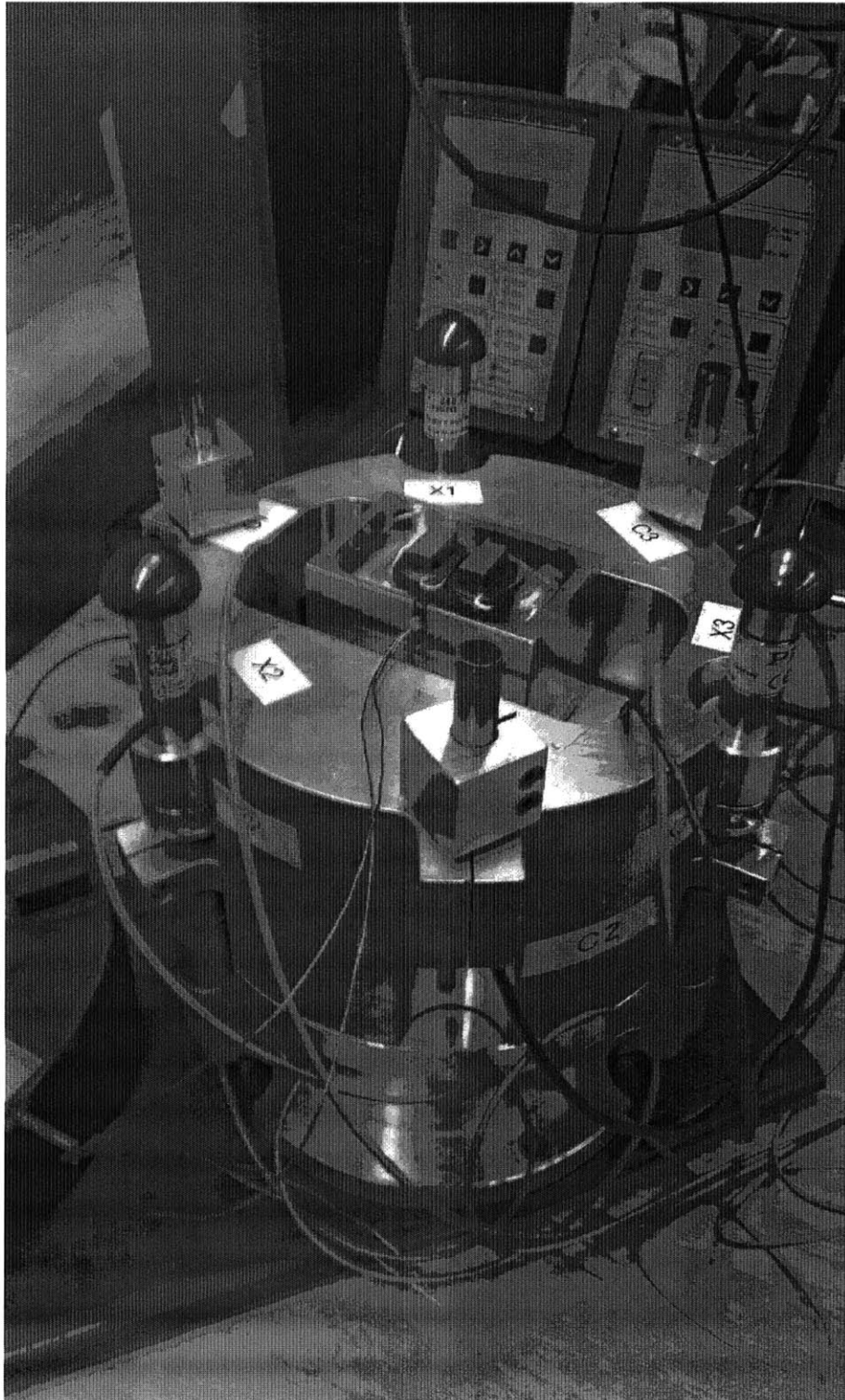


Figure 4-3: Gap Disturbance Testbed

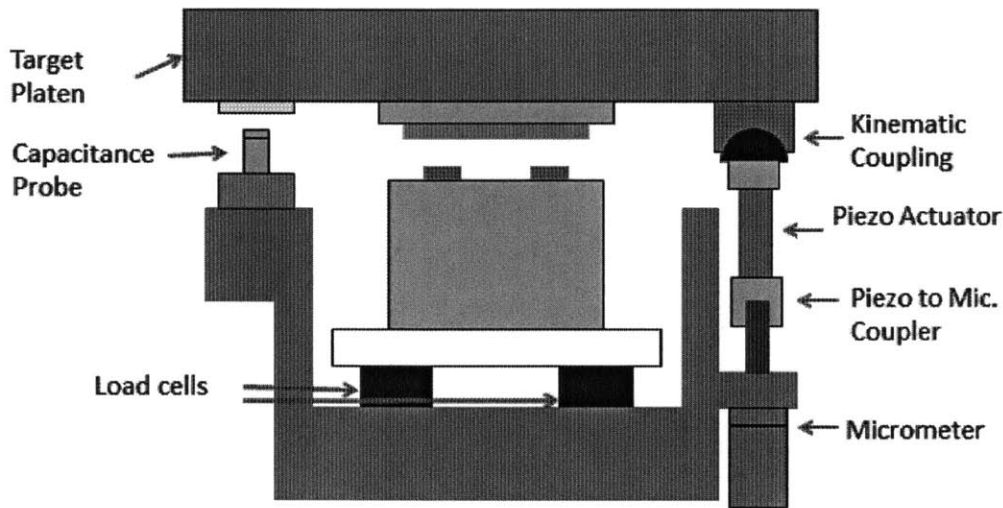


Figure 4-4: Cross section of Testbed with modifications

#### 4.2.1 Piezo Actuators

The piezo actuators were chosen so that their stroke, force and size would be appropriate for the experiments being conducted. A table of available piezos from Physik Instrumente (PI) is shown in Fig. 4-5. As mentioned in Chapter 2, the amplitude of the error in a lithographic Long Stroke is on the order of  $10\mu\text{m}$ . Given these considerations, the P840.10 from PI was chosen to be used for the experiment. The force limits from the piezo (on the order of hundreds of Newtons) far surpass the reluctance forces in the setup. The piezos are preloaded by using the same o-rings used to preload the kinematic coupling. The kinematic coupling ensures the piezos do not fight each other. The kinematic coupling is lubricated using a dry lubricant to minimize the frictional torques on the piezos.

In order to drive the piezo actuators, voltages of 60-100V are needed. Dedicated piezo amplifiers are very expensive (on the order of USD 1000-2000). For this project we decided on a cheaper alternative. Given the advent of haptic feedback in mobile phones, manufacturers have pushed for ICs to control these piezo-based haptic devices. One such IC is the DRV8662 from Texas Instruments. The DRV8662 includes

Model	P-841.1 P-840.1	P-841.2 P-840.2	P-841.3 P-840.3	P-841.4 P-840.4	P-841.5 P-840.5	Units
Open-loop travel @ 0 to 100 V	15	30	45	60	90	$\mu\text{m} \pm 20\%$
Closed-loop travel	15 / –	30 / –	45 / –	60 / –	90 / –	$\mu\text{m}$
Integrated feedback sensor*	SGS / –	SGS / –	SGS / –	SGS / –	SGS / –	
Closed-loop / open-loop resolution**	0.3 / 0.15	0.6 / 0.3	0.9 / 0.45	1.2 / 0.6	1.8 / 0.9	nm
Static large-signal stiffness***	57	27	19	15	10	$\text{N}/\mu\text{m} \pm 20\%$
Pushing forces to 1000 N	1000	1000	1000	1000	1000	N
Pulling forces to 50 N	50	50	50	50	50	N
Max. torque limit (on tip)	0.35	0.35	0.35	0.35	0.35	Nm
Electrical capacitance	1.5	3.0	4.5	6.0	9.0	$\mu\text{F} \pm 20\%$
Dynamic operating current coefficient (DOCC)	12.5	12.5	12.5	12.5	12.5	$\mu\text{A} / (\text{Hz} \cdot \mu\text{m})$
Unloaded resonant frequency $f_0$	18	14	10	8.5	6	$\text{kHz} \pm 20\%$
Operating temperature	-20 to +80	-20 to +80	-20 to +80	-20 to +80	-20 to +80	$^{\circ}\text{C}$
Mass without cables	20	28	46	54	62	$\text{g} \pm 5\%$
Material: case, end pieces	N-S	N-S	N-S	N-S	N-S	
Length L	32	50	68	86	122	$\text{mm} \pm 0.3$

Figure 4-5: Piezos Available from PI (taken from physikinstrumente.com)

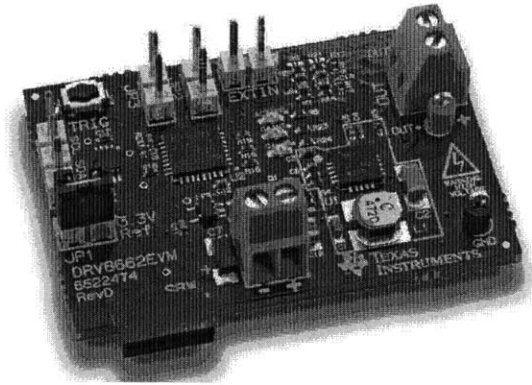


Figure 4-6: Evaluation Kit for DRV8662 Amplifier (image taken from Texas Instruments)

an integrated boost converter that can produce voltages up to  $\pm 100V$ . For this work we purchased 3 evaluation boards for the DRV8662. These evaluation boards break-out the QFN package of the DRV8662 into screw terminals which are more convenient to use. The evaluation board contains AC coupling capacitors in the analog input of the board which prevents the stock board from outputting any DC components. These AC-coupling capacitors (C4 and C5 in Figure 4-7) were shorted to allow for DC components to be produced and avoid any negative voltages getting applied to the piezos.

Special care must be used when dealing with mounting and dismounting piezos. In a first iteration of the piezo mount the adaptor was machined to sit flush with the top of the piezo. This was inadequate because it did not provide a way to insert a thin wrench to absorb the moment on the piezo when screwing on the kinematic coupling ball. This resulted in a broken piezo as shown in Fig. 4-8. The solution was to mount the adaptor in such a way that a thin wrench could be inserted to absorb the moment when tightening the piezo to the kinematic mount. Both ways of mounting the piezo are shown in Fig. 4-9.

### 4.2.2 Instrumentation

As in Poovey's experiments, the 3 DOFs of the platen are tracked using capacitance probes. The probes used in the study are ADE Technologies 4800 probes with a range





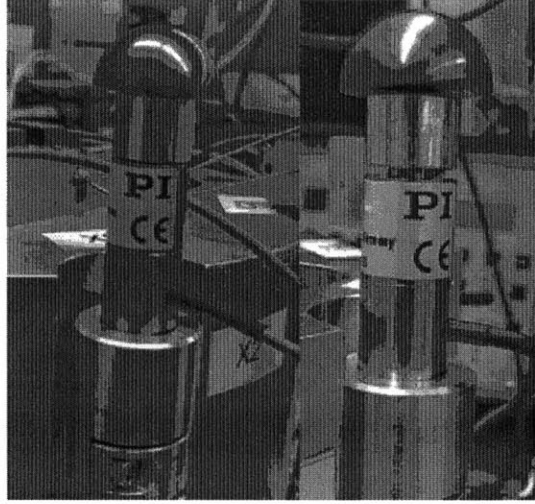


Figure 4-9: Two styles of mounting piezo adapter, notice the small gap on the right image allows for a thin wrench to be inserted when unscrewing the piezo

of 1mm. The output of these probes is run through a differential low pass RC filter to limit the bandwidth of the measurement. The break frequency of the RC filter is 1kHz.

The cap probes and kinematic mounts are arranged in a hexagon (the geometrical arrangement is shown in Fig. 4-10). Equation 4.1 gives the mapping from the cap probes (C1,C2,C3) to the kinematic coupling positions (X1,X2,X3). This mapping assumed all six point lie in one plane and that the platen suffers no deformation during experiments, this is a reasonable assumption given the forces the platen is subjected. This mapping is useful when setting the nominal gaps using the micrometers. The cap probe measurements also get converted to actuator coordinates namely, z position, pitch angle and roll angle (see figure 4-11 for the coordinate definition) . The transformation for these variables are shown in Equations 4.2-4.4.

$$\begin{bmatrix} C1 \\ C2 \\ C3 \end{bmatrix} = \begin{bmatrix} 2/3 & 2/3 & -1/3 \\ -1/3 & 2/3 & 2/3 \\ 2/3 & -1/3 & 2/3 \end{bmatrix} \begin{bmatrix} X1 \\ X2 \\ X3 \end{bmatrix} \quad (4.1)$$

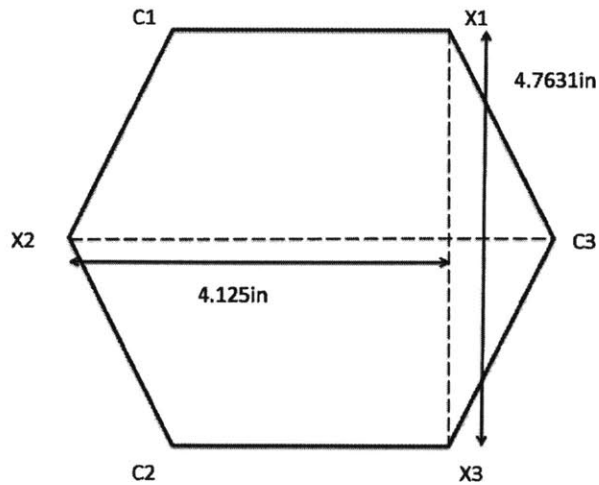


Figure 4-10: Hexagonal Arrangement of cap probes and kinematic mounts on target platten

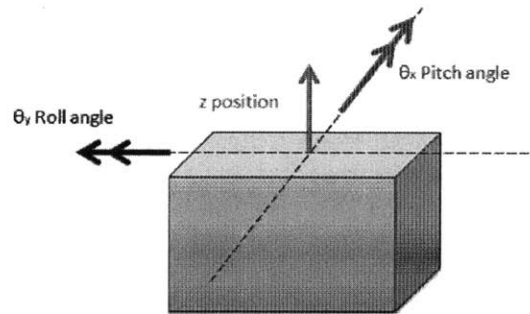


Figure 4-11: Coordinates with respect to reluctance actuator

$$z = \frac{C1 + C2 + C3}{3} \quad (4.2)$$

$$\theta_x = \frac{C2 - C3}{4.76\text{in} \times 25.4\text{mm/in}} \quad (4.3)$$

$$\theta_y = \left( C1 - \frac{C2 + C3}{2} \right) \frac{1}{4.125\text{in} \times 25.4\text{mm/in}} \quad (4.4)$$

The forces are measured using Kistler 9212 load cells. The load cells are connected to a charge amplifier which outputs an analog voltage. The sensitivity of the charge amplifier can be varied to accommodate the force levels that are being measured.

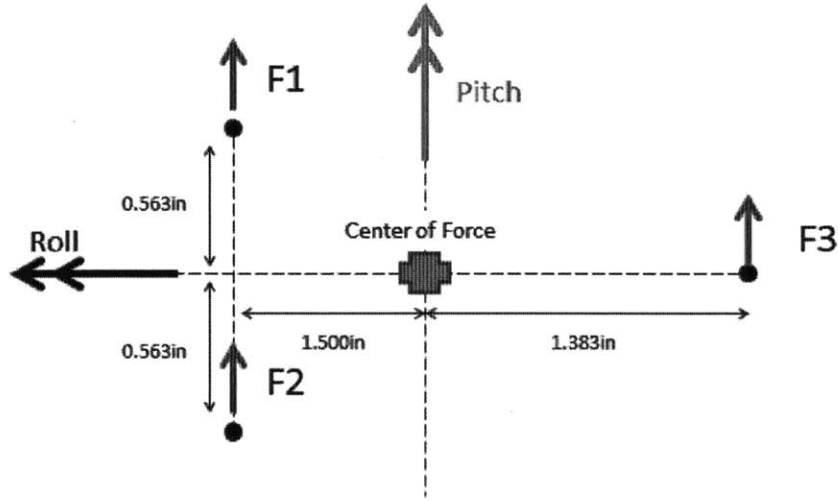


Figure 4-12: Geometry of Load Cell Positions

Figure 4-12 shows the arrangement of the load cells in the cavity. Each load cell is a single axis load cell and can measure tension and compression. The three signals from the load cells can be mapped to the normal force and the roll and pitch torque felt by the actuator. The total force on the actuator is simply the sum of the 3 forces on the load cells. While the torques are calculated using the lever arms shown in Fig. 4-12. Equations 4.5-4.7 show this matrix mapping.

$$F = F1 + F2 + F3 \quad (4.5)$$

$$T_{roll} = (F1 - F2) \times 0.563\text{in} \times 25.4\text{mm/in} \quad (4.6)$$

$$T_{pitch} = \left( \frac{(F1 + F2)}{2} \times 1.5\text{in} - 1.383\text{in} \times F3 \right) \times 25.4\text{mm/in} \quad (4.7)$$

### 4.2.3 Control Software

The signal acquisition and control all run on National Instrument hardware. An NI PXI 1031 chassis is connected to the host computer using an ethernet cable and all

the controllers and data acquisition run on this chassis in real time.

NI LabView is used as the control software. Various Virtual Instruments (VIs) were created and then deployed on the PXI chassis. The real time controller was run at a frequency of 10kHz.

# Chapter 5

## Experimental Results

This chapters presents the data taken from the test fixture.

### 5.1 Driving the Piezos

For simplicity the piezos were driven in an open-loop configuration, we fed a voltage to them and assumed the voltage was proportional to the displacement. This ignores the hysteresis in the piezo (which can be high (up to 20%) however because we are constantly monitoring the gap with capacitance probes we can use the real time measurement of the gap in our control algorithms. Also given the piezos are not put under high loads they result repeatable enough for our purposes. Fig. 5-1 shows the amplitude of gap oscillation corresponding to 3 excitation voltages.

Fig. 5-2 shows the effect of gap disturbance on the force measured by the load cells on an E-nickel actuator.

### 5.2 Calibration of Actuators

Before running any disturbance rejection experiments the actuators had to be calibrated. We ran a dynamic signal analysis (DSA) on both the U shaped Cobalt Actuator and the E shaped Nickel actuator (see Fig. 5-3). With this DSA we can then design a current controller for each actuator to use in the experiments. The DSA

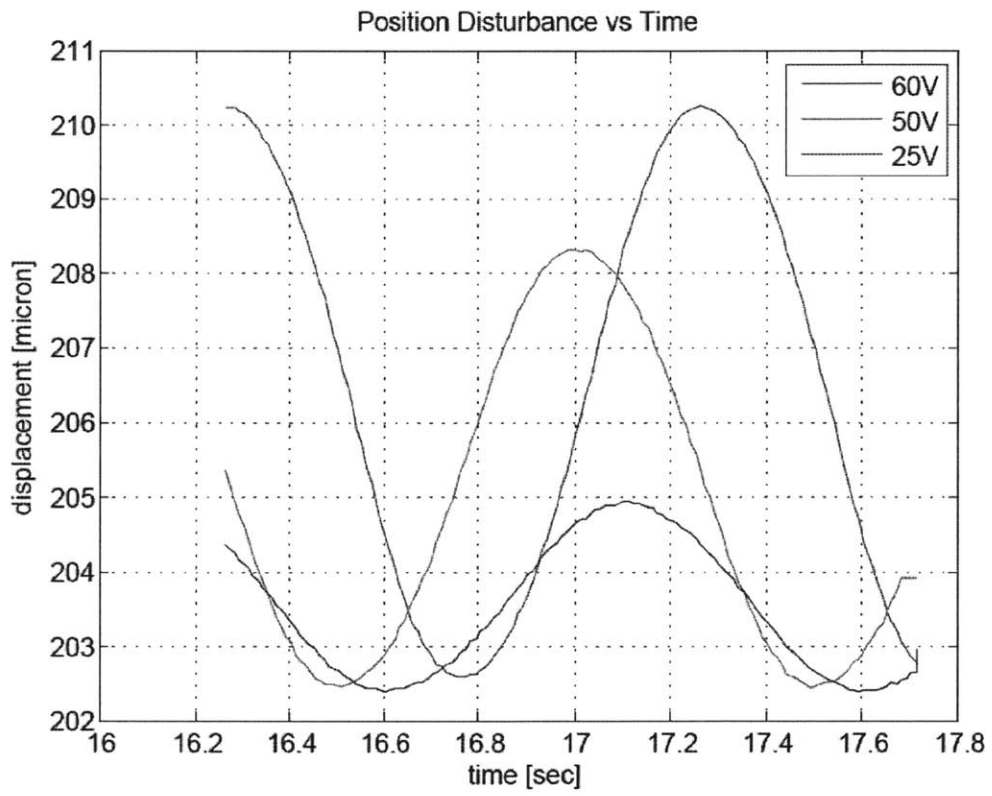


Figure 5-1: Stage response to Piezos at different voltage amplitudes.

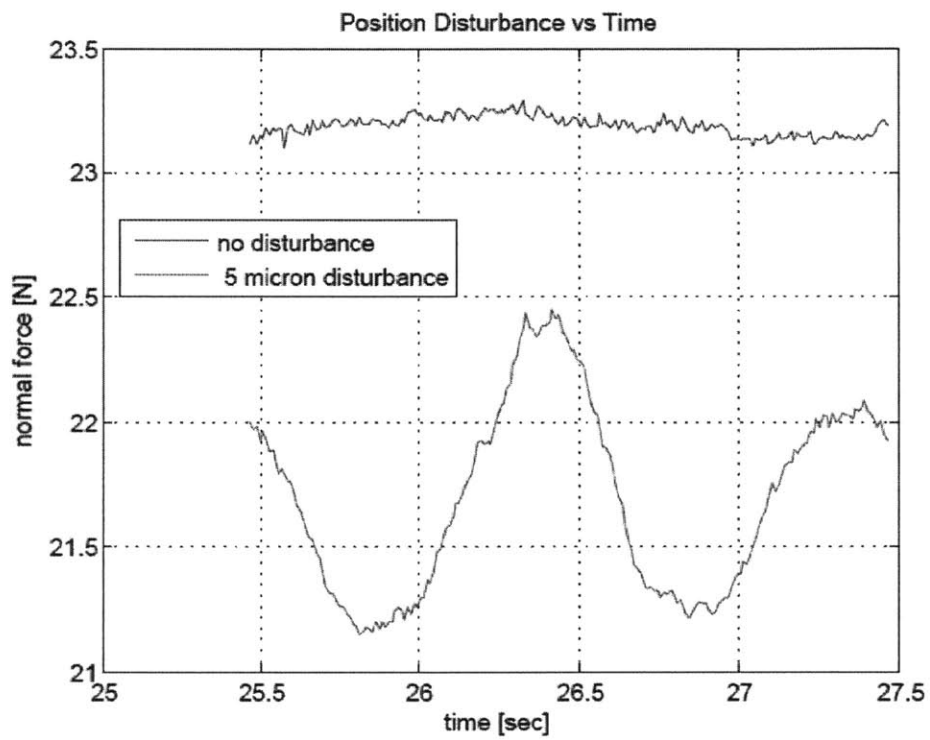


Figure 5-2: Disturbance in the force do to a 5 micron disturbance at 300 micron nominal gap (constant 1A current)

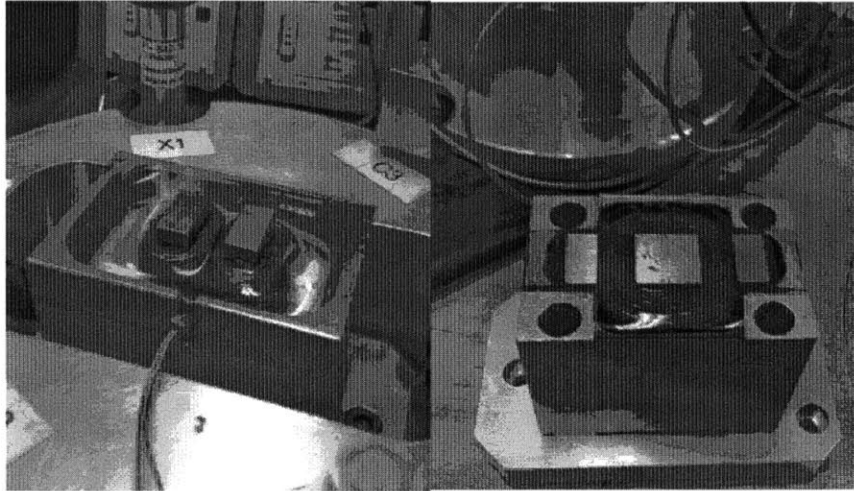


Figure 5-3: Cobalt Actuator (left) Nickel Actuator (right)

(and most experiments) were ran at a nominal gap of 300 micron. This gap was small enough for us to measure significant forces but also large enough so that the positive stiffness of the kinematic-coupled stage was still large enough in comparison to the magnetic negative stiffness and thus the nominal gap would stay relatively constant during operation.

The data from the DSA is shown in Fig. 5-4. The fit and compensated loop is shown in 5-5. The controller used is a PI controller.

With a current controller in place, the actuator force, current and gap relationships can be calibrated. Fig. 5-6 shows force current and gap data from the Nickel actuator.

We can now fit a quadratic profile to the curves, we don't use the 100 micron gap data because its very nonlinear and the experiments will not be happening at those small gaps. Fig. ?? shows the fitted profiles. Notice that the fit was optimized for 300 micron as most experiments will run at this nominal gap.

### 5.3 Disturbance Rejection via Feedforward

With the force-gap-current relationships in the actuators characterized, we can use feedforward to try and eliminate the stiffness in the actuator. This involves using the inverse of the quadratic model we fit to the curve and feeding the gap into a



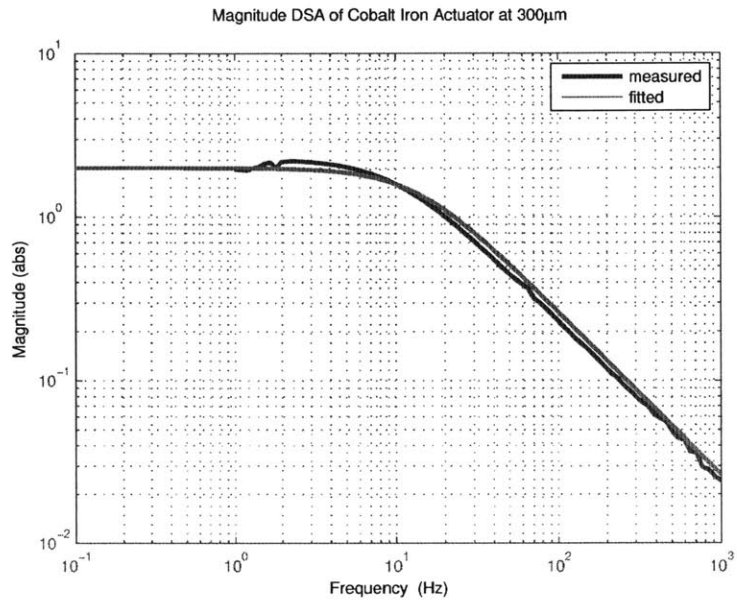


Figure 5-4: Dynamic signal analysis to determine cobalt actuator parameters at 300 $\mu$ m.

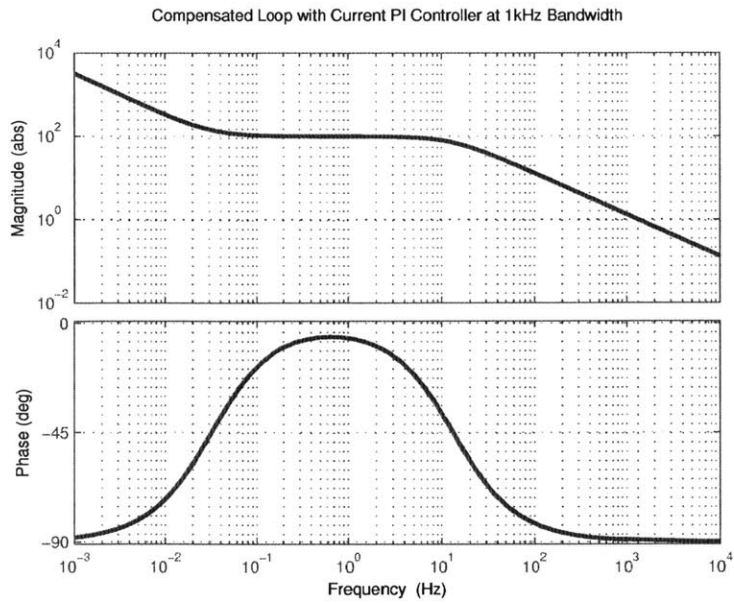


Figure 5-5: Compensated loop for the current controller in Cobalt Actuator.

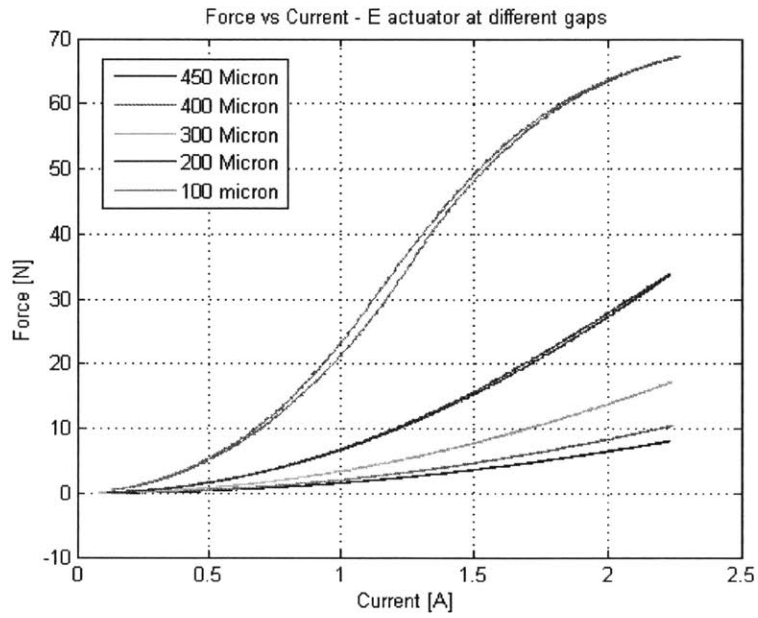


Figure 5-6: Force vs Current at different gaps for Nickel Actuator, notice the hysteresis and the saturation apparent in the 100 micron curve.

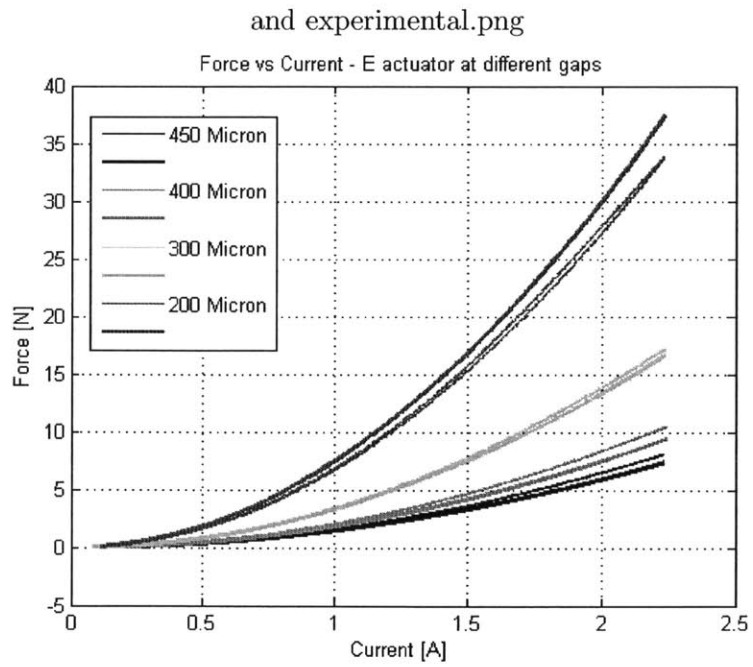


Figure 5-7: Force vs Current profiles fitted with a quadratic model.

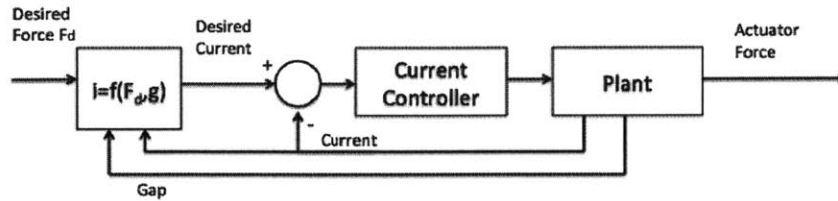


Figure 5-8: Feedforward control configuration.

nonlinear function before the controller in order to anticipate the current required by the actuator to generate a desired force. This is depicted in Fig. 5-8.

## 5.4 Flux Feedback

Chapter 3 discussed the form of flux feedback control used in this research. In order to be able to control the actuator effectively at a wide range of frequencies we need to run some calibration schemes to generate the required lookup tables (LUTs) to use in the flux control. To generate these LUTs the actuator current, gap, force, and sense coil voltage was recorded and then averaged. The current to flux mapping is shown in Fig. 5-9. notice that the loop has a width to it, this is because of hysteresis in the cobalt iron. The mapping from Force to Flux Linkage is shown in 5-10. Notice this mapping has no noticeable hysteresis to it given it maps flux to force directly, also notice the quadratic relationship that we expect from the Maxwell stress tensor.

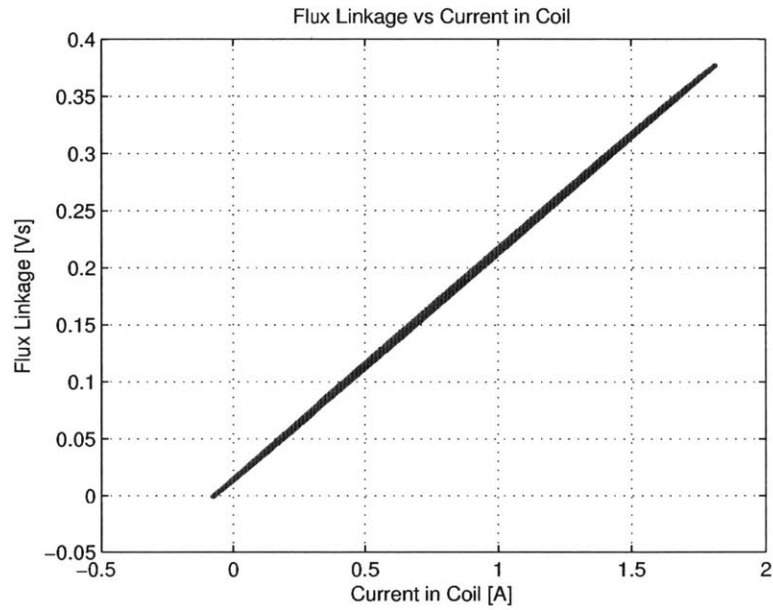


Figure 5-9: Flux linkage vs current in cobalt actuator at 300 micron gap, notice the width of the loop due to ferromagnetic hysteresis in the cobalt

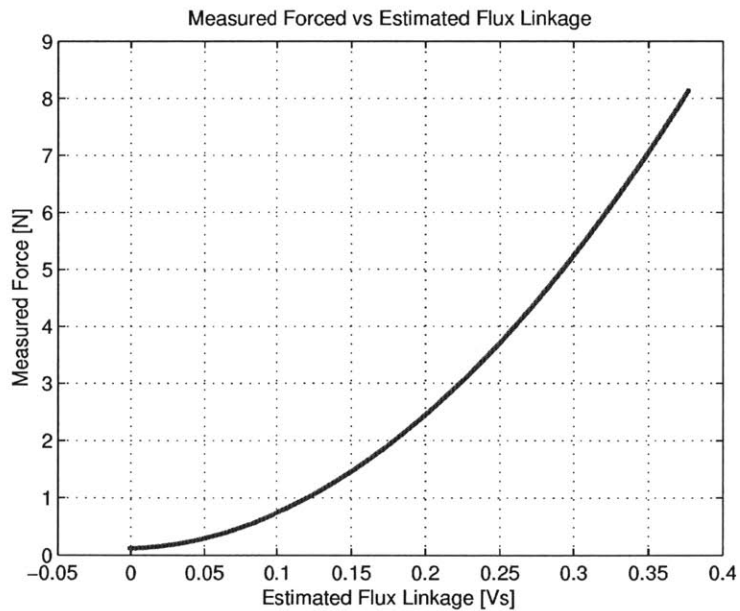


Figure 5-10: Force vs. Flux linkage in cobalt actuator at 300 micron gap, notice the quadratic relationship and the lack of noticeable hysteresis

# Chapter 6

## Conclusion and Future Work

This chapter summarizes the work and suggests directions for developing this research.

### 6.1 Summary of Work

In this thesis we have discussed the design and implementation of a variable dynamic gap test fixture for reluctance actuators. This testbed serves as a “scale model” on which to test reluctance actuator phenomena in the context of lithography stages. This thesis mainly focused on dealing with the gap disturbance and stiffness of such actuators. We also explored the issue of stray torques on the actuators.

In the design process we modified an existing test fixture to emulate phenomena that occur in a real photolithography system. We selected appropriate actuators to provide the right size and frequency spatial disturbances. We also used Finite Elements to achieve a first order description of the torsional negative stiffness of the actuator. we also implemented real time control techniques that allowed us to reject spatial disturbances and maintain a more accurate control of the force.

### 6.2 Suggestions for Further Research

This thesis act gives a first order pass on the parasitic torques coming from reluctance actuators. There is more research on this that is needed to expand the uses of

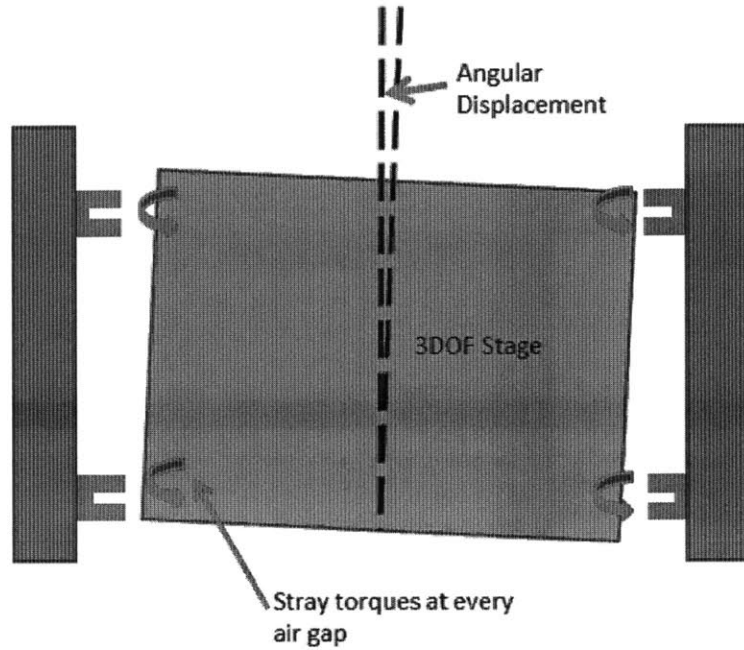


Figure 6-1: When multiple actuators are used in a stage configuration, the parasitic effects need to be compensated using active control in all DOFs.

reluctance actuators for positioning. Especially when we move forward to creating a 6 DOF stage driven by reluctance actuators. Such stage will need more accurate models of the torque parasitics of the actuators so that they can be controlled to meet accuracy specs. Fig. 6-1 shows a 3DOF example where the yaw controller must be able to reject the stray torques for each actuator.

As forces and accelerations on lithography stages keep increasing, the non-rigid modes of the stage will start getting excited and more actuators will be needed to maintain full controllability of the stage. Reluctance actuators are an attractive option to dampen these modes given they can be made more compact and are more efficient than their Lorentz counterparts. This concept is illustrated in Fig. 6-2.

This thesis only explored the use of a sense coil as feedback for the actuator. For further research it would be interesting to hybridize the sensing of the flux by using a hall effect sensor and a sense coil. This would eliminate the use of a look up table for the low frequency measurements, and also reduce the effect that magnetic hysteresis

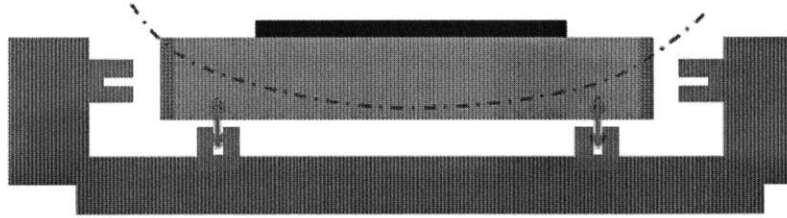


Figure 6-2: Reluctance Actuators are relatively compact to package in a stage, they can potentially be used for overactuation of a rigid body and dampen out the first couple of flexible modes for more complete control of the stage.

would have on the system. A possible implementation of such strategy could be obtained by sanding off the plastic packaging of a standard hall effect sensor so that it does not compromise the gap as much as illustrated on Fig. ???. With the continuous improvement of MEMS based sensors it is also not implausible that soon enough a very thin Hall Effect Sensor could be made available for better flux sensing.

This thesis showed that the smaller the gap that is being handled by the reluctance actuator, the efficiency of the actuator increases. Ultimately this benefit is limited by the mechanical stiffness of the mounting of the actuators. In [2] gaps on the order of millimeters are used. Given the travel of the Short stroke does not exceed 500 microns, in theory it is possible to reduce the operating gaps at which the stage is run. Further research in the integration of these actuators should aim to stiffen the system in order to get the smallest operating gap possible.

The experimental setup in this thesis was not stiff enough to perform accurate force control experiments with gaps on the order of 100-150 microns. Fig. ??? shows how the nominal gap changes by a significant amount when increasing the current to the actuator. This flexing is thought to come from the kinematic couplings and the piezos. If these actuators are to be used below gaps of 200 microns there has to be a stiffer mounting solution for effectively utilizing the actuators in a stage configuration.

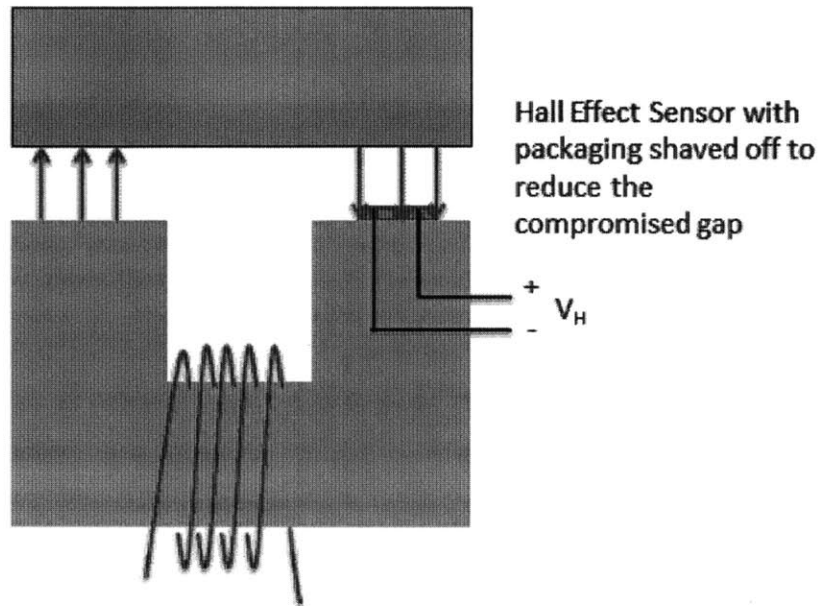


Figure 6-3: Package-less Hall Effect Sensors could lead to better flux sensing without too much air gap loss.

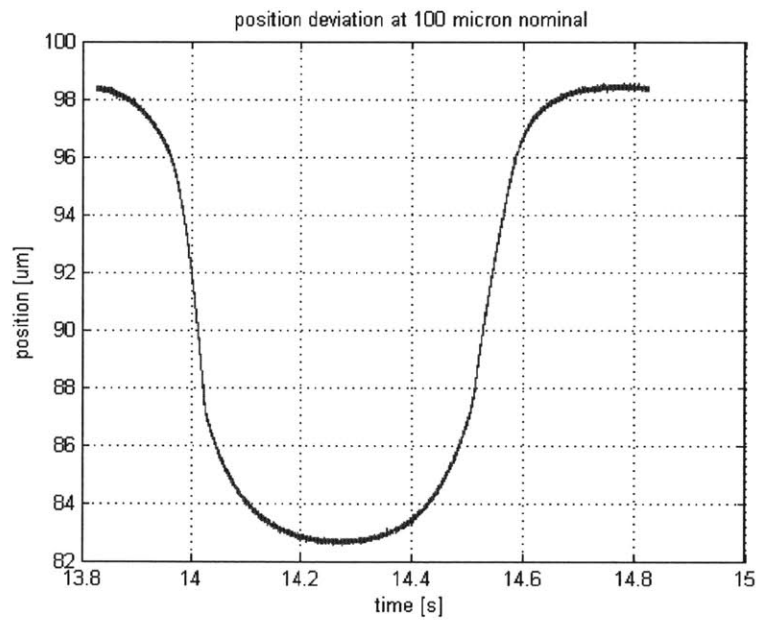


Figure 6-4: Deformation of stage when a 2 Amp peak sine wave is passed through the actuator.



# Bibliography

- [1] H. Butler. Position control in lithographic equipment. *IEEE Control Systems Magazine*, 41(7):73+, 2011.
- [2] Fluke. Fluke insulation multimeters, May 2014.
- [3] Katalenic. *Design and control methods for high-accuracy variable reluctance actuators*. PhD dissertation, Eindoven, 2013.
- [4] Ian MacKenzie. *Design and control methods for high-accuracy variable reluctance actuators*. PhD dissertation, Massachusetts Institute of Technology, 2014.
- [5] David Meeker. Finite element method magnetics, May 2013.
- [6] James R. Melcher. *Continuum Electromechanics*, chapter 1.2. MIT Press, 1981.
- [7] Tony L. Poovey. A kinematically coupled magnetic bearing test fixture. Master's thesis, University of North Carolina at Charlotte, 1992.
- [8] Adrian Toma. Reluctance vs lorentz. *Mikroniek*, 2013.
- [9] David L. Trumper. Linearizing control of magnetic suspension systems. *IEEE Transactions on Control Systems Technology*, 5(4):427+, 1997.
- [10] Vacuumschmelze. ferromagnetic materials, May 2010.